Earth Science Faculty Scholarship   Earth Sciences

11-15-2003

Geometrical Force Balance in Glaciology

Terence J. Hughes

University of Maine - Main, terry.hughes@maine.edu

Geometrical force balance in glaciology

T. Hughes

Department of Earth Sciences, Climate Change Institute, Bryand Global Sciences Center, University of Maine, Orono, Maine, USA

[1]   The analytical force balance traditionally used in glaciology relates gravitational forcing to ice surface slope for sheet flow and to ice basal buoyancy for shelf flow. It is unable to represent stream flow as a transition from sheet flow to shelf flow by having gravitational forcing gradually passing from being driven by surface slope to being driven by basal buoyancy downslope along the length of an ice steam. This is a serious defect, because ice streams discharge up to 90% of ice from ice sheets into the sea. The defect is overcome by using a geometrical force balance that includes basal buoyancy, represented by the ratio of basal water pressure to ice overburden pressure, as a source of gravitational forcing. When combined with the mass balance, the geometrical force balance provides a holistic approach to ice flow in which resistance to gravitational flow must be summed upstream from the calving front of an ice shelf. This is not done in the analytical force balance, and it provides the ice-thinning rate required by gravitational collapse of ice sheets as interior ice is downdrawn by ice streams.   *INDEX TERMS:* 1645 Global Change: Solid Earth; 1863 Hydrology: Snow and ice (1827); 1827 Hydrology: Glaciology (1863); 3210 Mathematical Geophysics: Modeling; *KEYWORDS:* glaciology, geometrical force balance, ice, flow

1.   Introduction

[2]   A holistic approach to ice sheet modeling, based on a geometric force balance, is presented to show how ice sheets can trigger rapid climate change by undergoing large, rapid changes in size and shape that radically alter climatic equilibrium. This approach departs from that by *Hughes* [1992, 1998] by including ice thinning or thickening over time, and by extending the solution to ice flow that may or may not end in water.

[3]   Ever since *Orowan* [1949] took the first step in transforming glaciology from a descriptive branch of geology into a quantitative branch of physics, an underlying assumption has been that glacial flow can be quantified adequately by balancing local forces at a point. Specifically, a gravitational driving force proportional to the product of ice thickness and ice surface slope induces downslope ice motion that is resisted primarily by the shearing force at the bed, and secondarily by shearing forces along the sides of a flowband and longitudinal extending or compressive forces along the length of the flowband [*Nye*, 1951]. It is known that side shear is negligible for slow uniform "sheet flow" in continental ice sheets [*Nye*, 1959], but can exceed basal shear in ice streams, which are fast currents of ice that drain up to 90% of ice sheets [e.g., *Hughes*, 1977; *Echelmeyer et al.*, 1994; *Whillans and Van der Veen*, 1997]. Longitudinal forces were considered to arise primarily from changes in the surface mass balance, bed topography, and ice-bed coupling [e.g., *Van der Veen*, 1999, pp. 236–244]. That

all of these forces could be balanced locally remained an underlying assumption of ice sheet dynamics after *Mahaffy* [1976] showed how one-dimensional flowband models could be converted into two-dimensional grid point models in the map plane. Map-plane models typically balance the local gravitational force against only the local basal shear force at grid points [e.g., *Budd et al.*, 1984; *Fastook*, 1992; *Huybrechts*, 1990, 1994; *Greve*, 1997].

[4]   Challenges to this assumption began when *Thomas* [1973a, 1973b] showed that "shelf flow" in floating ice shelves could be severely retarded by shear along the sides of embayments that confine an ice shelf and by shear over or around sites of local grounding which produce ice rumples or ice rises, respectively, on the surface of an ice shelf. These resisting forces could not balance gravitational forces locally because they exerted a cumulative effect from the calving front to the grounding line of a given ice-shelf flowband. This was the first demonstration that a holistic approach was needed in modeling flow of ice shelves, an approach used by *Thomas and MacAyeal* [1982] in force balance calculations at a grid-like set of locations on the Ross Ice Shelf in Antarctica. The "back force" resisting gravitational forcing at each grid point was determined by subtracting the observed ice velocities from those calculated using the *Weertman* [1957a] expression for an unconfined ice shelf.

[5]   A challenge to the assumption that a local balance of forces was adequate to describe ice sheet dynamics was presented by *Hughes* [1992] on the grounds that ice streams discharged up to 90% of ice from ice sheets, that stream flow was transitional between sheet flow and shelf flow, and that a

holistic approach to ice stream dynamics was needed to describe the transition. The centerpiece of this holistic approach was a geometrical force balance in which, for a given ice thickness, gravitational forcing was controlled mainly by ice surface slope at the head of an ice stream and mainly by ice height above water when the ice stream becomes afloat. Ice height above water was controlled by basal buoyancy so gravitational forcing for ice stream dynamics could be represented by a transition from surface slope to basal buoyancy along the downstream length of an ice stream. Resistance to gravitational forcing was provided not only by the ''back forces'' in the ice shelf beyond the ice stream, but also by basal shear, side shear, and longitudinal extension or compression, all summed cumulatively upstream along the ice stream. This is the holistic approach. Other holistic approaches to modeling ice streams that indirectly invoked basal buoyancy were developed by *MacAyeal* [1989] and *Hulbe and MacAyeal* [1999].

[6] The geometrical force balance, unlike an analytical force balance, allows gravitational forcing at each point along a flowband or in a map-plane grid of points to be partitioned between contributions from surface slope and basal buoyancy, as represented by the ratio of basal water pressure P_W to ice overburden pressure P_I. This partitioning is represented by the difference in areas of triangles whose areas are the gravitational force per unit width of a flowband. Partitioning can be determined only if all downstream forces resisting stream flow are calculated and summed from the calving front to the grounding line of an ice shelf and then up the ice stream supplying the ice shelf. In this holistic approach, reductions of downstream resisting forces, notably disintegration of the buttressing ice shelf, can be transmitted almost instantaneously up an ice stream and result in accelerated downdraw of interior ice and gravitational collapse of the ice sheet [*Hughes*, 1986, 1998, pp. 7–11]. Reliance on only a local balance of forces will not deliver these positive feedbacks, and leads to the unwarranted conclusion that ice sheets respond only slowly and passively to climate change through changes in their mass balance. In fact, ice sheets may trigger climate change by rapid collapse and discharge of ice driven by inherent internal positive feedback mechanisms [*Heinrich*, 1988; *Andrews and Tedesco*, 1992].

[7] Demonstrating the capacity of ice sheets to undergo rapid changes that might give rise to rapid climate change is not the goal of this investigation. Rather, it is to lay the foundation upon which a demonstration might be based. Sections 2 through 5 review conventional glaciological treatments for gravitational thinning rates of free and confined ice shelves. Sections 6 through 8 extend these treatments to include thinning of ice streams in a geometrical force balance.

[8] Section 2 shows how the linear increase with depth through ice of longitudinal and vertical stresses σ_{xx} and σ_{zz} can be represented by triangles, with the difference in area of triangles being the respective longitudinal gravitational forces per unit flowband width for shelf flow and for sheet flow. Section 3 shows how ice-thinning rates along the flowband are related to the mass balance and the longitudinal strain rate for transitions from sheet flow to stream-flow to shelf flow. Section 4 introduces basal buoyancy into the force balance for fully buoyant freely floating ice,

calculates the longitudinal buoyancy force, and converts it into a longitudinal deviator stress. The flow law of ice is then used to convert that stress into the longitudinal strain rate in the mass balance. Section 5 combines the mass balance in section 3 with the longitudinal strain rate in section 4 to obtain the ice thickness gradient of an ice shelf along a flowband from its calving front back to its grounding line. It includes the effect of resistance from side shear, which is then converted into a longitudinal compressive stress that opposes the gravitational longitudinal extending stress.

[9] Section 6 introduces basal buoyancy factor P_W/P_I for ice streams. It can increase from nearly zero to nearly one downstream, and it reduces the longitudinal deviator stress for shelf flow. Its corresponding longitudinal strain rate is combined with the mass balance and stresses resisting flow to give the typically concave surface of stream flow. This concave surface is transitional from the convex surface of sheet flow as $P_W/P_I \to 0$ to the flat surface of shelf flow as $P_W/P_I \to 1$. Section 7 shows how the geometrical force balance is related to the traditional analytical force balance. The two are the same, but the geometrical force balance relates the longitudinal deviator tensile stress to P_W/P_I. Section 8 is more speculative and concludes the study. It discusses how variations of P_W/P_I might allow the concave surface of an ice stream to become the convex profile of an ice lobe if it ends on land instead of in water, and how P_W/P_I might trigger gravitational collapse of an ice sheet or halt collapse.

2. A Geometrical Representation of Gravity Forces

[10] A geometrical representation of longitudinal gravitational forcing is illustrated in Figure 1. It shows that for both floating and grounded ice, gravitational motion by horizontal spreading along x and vertical thinning along z occurs because horizontal stress σ_{xx} is slightly less compressive than vertical stress σ_{zz}, so that $\sigma_{xx} - \sigma_{zz}$ is a tensile longitudinal deviatoric stress σ_T that deviates from the hydrostatic (lithostatic for ice) state of stress for which there is no ice motion. For ice thickness h_I in Figure 1, the longitudinal gravitational driving force along x per unit transverse width of ice along y is the shaded area that lies between the sloping lines showing the respective increase of σ_{xx} and σ_{zz} with depth through the ice for both floating and grounded ice. With $\sigma_{yy} = \sigma_{zz}$, so transverse strain rate $\dot{\epsilon}_{yy} = 0$, Figure 1 represents a plane-strain condition. For floating ice with a draught h_W below water, the shaded area results from an ice elevation of height $h_I - h_W$ floating above water, and this gravitational force is balanced by the tensile force h_I $(\sigma_{xx} - \sigma_{zz})$, both being forces per unit width of ice. For grounded ice, the shaded area results from a change Δh in ice elevation along horizontal distance Δx because grounded ice has a surface slope $\Delta h/\Delta x$, with $\Delta h = \Delta h_I$ for a horizontal bed. This produces a tensile gravitational force h_I $(\sigma_{xx} - \sigma_{zz}) = -h_I \Delta \sigma_{zz}$ that is balanced by a basal drag force $\tau_O \Delta x$, where τ_O is the basal shear stress in ice, and $\Delta \sigma_{zz}/\Delta x$ remains finite as $\Delta x \to 0$. As with floating ice, these are forces per unit width of ice. The force balance in both cases is obtained by using the difference in area of triangles formed from the linear increase of compressive
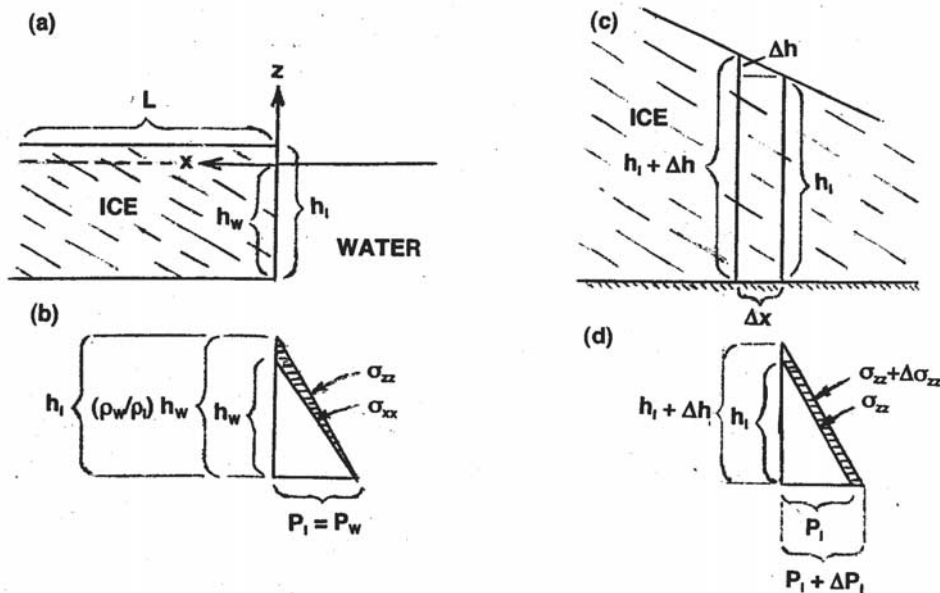
Figure 1. A geometrical representation of gravitational forcing in floating and grounded ice. (a) Floating ice having constant thickness. (b) The gravitational driving force per unit width of ice is the shaded area between the increase with depth of compressive stresses σ_{zz} and σ_{xx} for floating ice. (c) Sloping ice grounded on a horizontal bed. (d) The gravitational driving force per unit width of ice is the shaded area between compressive stresses $\sigma_{zz} + \Delta\sigma_{zz}$ and σ_{zz} for grounded ice over incremental upslope length Δx. In this and subsequent figures, the shaded areas in Figures 1b and 1d are the horizontal gravitational force per unit width. Vertical distributions of these areas do not cause vertical variations in horizontal strain rate $\dot{\varepsilon}_{xx}$. The size of the shaded areas in Figures 1b and 1d are important, not their shape. The same is true of the shaded areas in Figures 2, 3, 4, and 6. To emphasize that $\dot{\varepsilon}_{xx}$ is constant through the ice thickness, all these shaded areas could be replaced by rectangles having the same area and a constant width, representing longitudinal deviator stress, in the z direction.

stresses σ_{xx} and σ_{zz} with depth through the ice. This difference is caused by basal buoyancy for floating ice and by surface slope for grounded ice. It provides a geometrical force balance based on representing gravitational forcing by the areas of triangles. It was used explicitly by *Robin* [1958] in his treatment of ice-shelf spreading and implicitly by *Nye* [1952] in his treatment of ice-sheet spreading.

[11] A danger of the geometrical force balance shown in Figure 1 and subsequent figures is that it creates the false impression that $\sigma_{xx} - \sigma_{zz}$ varies through the ice thickness, so that longitudinal strain rate $\dot{\varepsilon}_{xx}$ varies vertically. Neither is true. Both $\sigma_{xx} - \sigma_{zz}$ and $\dot{\varepsilon}_{xx}$ are constant in the z direction. To make this point, the shaded triangle that represents $\sigma_{xx} - \sigma_{zz}$ should be replaced by a rectangle having constant $\sigma_{xx} - \sigma_{zz}$ along z and having the same area as the triangle. This would emphasize that the size of the shaded area is the important feature in the geometrical force balance, not the shape of the shaded area.

[12] Ice streams discharge upwards of 90% of ice into the sea for both the ice sheets of Greenland and Antarctica. Ice streams are therefore the primary vehicles by which an ice sheet becomes an ice shelf. This "march to the sea" is, of course, offset by precipitation over the ice sheets that continually supplies new ice, so that ice lost by the force balance is returned in greater or lesser measure by the mass balance, causing the ice sheets to grow or shrink. Since

stream flow is the primary vehicle by which sheet flow becomes shelf flow, the gravitational driving force for ice streams should involve both the surface slope and basal buoyancy of ice, with surface slope dominating at the head of an ice stream where sheet flow becomes stream flow, and basal buoyancy dominating at the foot of an ice stream where stream flow becomes shelf flow. This was done by combining the mass balance with a geometrical force balance [*Hughes*, 1992]. However, most glaciologists still use only the ice surface slope when treating sheet flow and stream flow, reserving basal buoyancy only for treatments of shelf flow. This is a fundamental defect in glaciology because it ignores a major component of gravitational forcing by which ice sheets discharge ice into the sea.

[13] An attempt to correct this defect is made by first writing the equation for mass balance in a way that emphasizes the longitudinal strain rate $\dot{\varepsilon}_{xx}$, since it arises from ice flow produced by the stress difference $\sigma_{xx} - \sigma_{zz}$. Then the geometrical force balance is applied to longitudinal spreading of a tabular iceberg, an ice shelf grounded at one end, an ice shelf grounded at one end and along both sides, and an ice stream that supplies the ice shelf. This approach illustrates the power of the geometrical force balance as it is applied from the most simple to the most complex glacial system. Unlike earlier applications of the geometrical force balance [*Hughes*, 1996, 1998], ice thinning or thickening over time is also included in this

application. Advantages of this approach are discussed and appropriate conclusions are drawn.

3.   Mass Balance for Longitudinal Creep in Ice

[14] An ice sheet generally creeps by longitudinal extension in the accumulation zone and by longitudinal compression in the ablation zone as it responds to the mass balance. In the mass balance, ice has thickness h_I at distance x from the origin of axes x, y, z, with x and y in horizontal directions, x positive against ice flow and y positive abeam of ice flow, and z positive upward in the vertical direction. In this treatment, x is positive toward the center of ice spreading, and follows ice flowbands having variable width w_I. The mass balance for constant ice accumulation rate a, variable ice thickness h_I, and ice velocity u_x (negative u_x because ice flows in the minus x direction) must allow for an ice thickening (positive) or thinning (negative) rate of

$$dh_I/dt = a + h_I\dot{\varepsilon}_{zz} - u_x dh_I/dx$$
$$= a - h_I\left(1 + \dot{\varepsilon}_{yy}/\dot{\varepsilon}_{xx}\right)\dot{\varepsilon}_{xx} - u_x dh_I/dx, \qquad (1)$$

where $\dot{\varepsilon}_{xx}$, $\dot{\varepsilon}_{yy}$, and $\dot{\varepsilon}_{zz}$ are respective longitudinal, transverse, and vertical strain rates such that $\bar{\varepsilon}_{xx} + \bar{\varepsilon}_{yy} + \bar{\varepsilon}_{zz} = 0$ in order to conserve ice volume, and dh_I/dx is the ice thickness gradient. Strain rates are related to velocity gradients as follows:

$$\dot{\varepsilon}_{ij} = 1/2\left(\partial u_i/\partial j + \partial u_j/\partial i\right), \qquad (2)$$

with indices i, $j = x$, y, z in all combinations according to standard tensor notation. Mass balance conservation also requires that for a flowband of variable width w_I at upstream distance x, where $w_I = w_O$, $h_I = h_0$, and $u_x = u_0$ at $x = 0$, for average width $\bar{w}_I$ and average thickening or thinning rate $d\bar{h}_I/dt$ along x, assuming $d\bar{w}_I/dt \ll d\bar{h}_I/dt$ and can be ignored,

$$\int_O^x \bar{w}(\partial h/\partial t)dx \approx \left(d\bar{h}_I/dt\right)\bar{w}_I x = a\bar{w}_I x - (w_I h_I u_x - w_0 h_0 u_0). \quad (3)$$

In applications of equation (3) used here, $x = 0$ is at the ice-shelf calving front, as required in a holistic approach, and where w_0, h_0, and u_0 are relatively easy to measure.
[15] Combining equations (1) and (3), and solving for ice thickness gradient dh_I/dx,

$$\frac{dh_I}{dx} = \frac{w_I h_I\left[(a - dh_I/dt) - h_I\left(1 + \dot{\varepsilon}_{yy}/\dot{\varepsilon}_{xx}\right)\dot{\varepsilon}_{xx}\right]}{(a - d\bar{h}_I/dt)\bar{w}_I x + w_0 h_0 u_0}. \qquad (4)$$

If flowband width w_I changes an incremental amount Δw_I over incremental length Δx, where equation (2) gives $\dot{\varepsilon}_{xx} = \Delta u_x/\Delta x$ for incremental velocity change Δu_x along Δx, then $\dot{\varepsilon}_{yy} = (\Delta w/w)\bar{u}_x/\Delta x$ for mean velocity $\bar{u}_x$ along Δx. In equation (4),

$$\frac{\dot{\varepsilon}_{yy}}{\dot{\varepsilon}_{xx}} = \frac{(\Delta w_I/w_I)\bar{u}_x/\Delta x}{\Delta u_x/\Delta x} = \frac{\Delta w_I \bar{u}_x}{w_I \Delta u_x}. \qquad (5)$$

[16] Equation (4) applies for sheet flow, stream flow, and shelf flow. For one-dimensional linear flow, $w_O = w_I = \bar{w}_I$,

and $\dot{\varepsilon}_{yy} = 0$. For mass balance equilibrium, $\partial h_I/\partial t = \partial \bar{h}_I/\partial t = 0$ and equation (4) becomes

$$\frac{dh_I}{dx} = \frac{h_I(a - h_I\dot{\varepsilon}_{xx})}{ax + h_0 u_0}. \qquad (6)$$

For shelf flow that can diverge and converge along x, the ice slab in Figure 1 creeps uniformly to the right and left so that $dh_I/dx = 0$, and equation (4) becomes

$$dh_I/dt = a - h_I\left(\dot{\varepsilon}_{xx} + \dot{\varepsilon}_{yy}\right) = a + h_I\dot{\varepsilon}_{zz}. \qquad (7)$$

When the ice slab in Figure 1 is a tabular iceberg, $\dot{\varepsilon}_{xx} = \dot{\varepsilon}_{yy} = -1/2\dot{\varepsilon}_{zz}$.

4.   Force Balance for Creep of Buoyant Ice

[17] The vertical force balance at the base of the ice slab in Figure 1 requires that a downward gravitational body force F_B is offset by an upward compressional force F_C such that

$$F_B - F_C = m_I g_z - P_I A_z = \rho_I h_I A_z g_z - P_I A_z = 0, \qquad (8)$$

where m_I is the ice mass, ρ_I is ice density, A_z is the basal area of the ice slab over length x and width w_I, g_z is the vertical acceleration vector due to gravity, and P_I is the ice overburden pressure at the base of the slab. The vertical force balance for an equivalent mass m_W of water is

$$F_B - F_C = m_W g_z - P_W A_z = \rho_W h_W A_z g_z - P_W A_z = 0, \qquad (9)$$

where ρ_W is water density. In equations (8) and (9), area $A_z = w_I x$ is a vector in the z direction and gives the direction of vertical forces F_C. Equations (8) and (9) give

$$P_I = \rho_I g h_I, \qquad (10a)$$

$$P_W = \rho_W g h_W, \qquad (10b)$$

$$\frac{P_W}{P_I} = \frac{\rho_W h_W}{\rho_I h_I}, \qquad (10c)$$

where gravity is now represented by the scalar g because P_W and P_I are scalars. For ice having full, partial, and no support from basal buoyancy, $P_W/P_I = 1$, $0 < P_W/P_I < 1$, and $P_W/P_I = 0$, respectively. Ratio P_W/P_I is therefore a measure of ice-bed coupling. For the floating ice slab in Figure 1, $P_W/P_I = 1$ so $h_I = (\rho_W/\rho_I) h_W$ is the buoyancy condition. The gravitational driving force in Figure 1 arises from ice height $h = h_I - h_W$ above water for shelf flow, compared to ice-height change Δh in length Δx for sheet flow, where $\alpha = \Delta h/\Delta x$ is the local ice surface slope as $\Delta x \to 0$. Note that ice height h is elevation above sea level, whereas ice thickness h_I is elevation above the bed. In both cases, ice moves in the horizontal direction to displace air. The horizontal force balance for the floating ice slab can be performed at either end of the slab, where average ice pressure $\bar{P}_I = 1/2 P_I$ on area $(A_x)_I = w_I h_I$ of ice is only partly offset by average water pressure $\bar{P}_w = 1/2 P_W$ on area $(A_x)_W =$

$w_I h_W$ of water, so the force balance requires a deviatoric tensile stress σ_T on area $(A_x)_I$,

$$\bar{P}_I (A_x)_I - \bar{P}_W (A_x)_W - \sigma_T (A_x)_I = 0. \qquad (11)$$

Substituting for $\bar{P}_I$ and $\bar{P}_W$ using equations (10a) and (10b) for P_I and P_W,

$$(1/2 \rho_I g h_I) w_I h_I - (1/2 \rho_W g h_W) w_I h_W - \sigma_T w_I h_I = 0. \qquad (12)$$

Applying the geometrical force balance, the first two terms are the difference in areas of the force triangles for the floating ice slab in Figure 1. Areas $(A_x)_I$ and $(A_x)_W$ are unequal positive and negative horizontal vectors that make σ_T positive (tensile), since $\bar{P}_I$ and $\bar{P}_W$ are scalars and $\bar{P}_I = \bar{P}_W$ for buoyant ice. Solving equation (12) for σ_T,

$$\sigma_T = 1/2 \rho_I g h_I (1 - \rho_I / \rho_W). \qquad (13)$$

Equation (13) was first derived by *Weertman* [1957a]. As seen in Figure 1, σ_T is tensile because pressure P in the ice slab is the average of compressive stresses, σ_{xx}, σ_{yy}, and σ_{zz}, where $\sigma_{yy} = \sigma_{zz}$ but $\sigma_{xx} < \sigma_{zz}$ for linear flow along x because stretching of ice by strain rate $\dot{\varepsilon}_{xx}$ makes σ_{xx} less compressive than σ_{yy} and σ_{zz}. According to the flow law of ice, using the standard tensor notation [*Nye*, 1953],

$$\dot{\varepsilon}_{ij} = (\sigma_e^{n-1} / A^n) \sigma'_{ij}, \qquad (14)$$

where n is a viscoplastic creep parameter such that $n = 1$ for viscous creep and $n = \infty$ for plastic creep, A is an ice hardness parameter that depends on ice temperature and crystal fabric, σ_{ij}^t is a deviator stress that causes creep deformation, and σ_e is an effective creep stress that is related to the second invariant of deviator stresses $1/2\sigma_{ij}^t \sigma_{ji}^t$ such that $2\sigma_e^2 = \sigma_{ij}^t \sigma_{ji}^t$. Since σ_{kk} is the first invariant of applied stresses σ_{ij}, such that $\sigma_{kk} = 3P$, flow is caused by deviator stresses σ_{ij}^t that deviate from the lithostatic and hydrostatic spherical symmetry of P for ice and water,

$$\sigma'_{ij} = \sigma_{ij} - 1/3 \delta_{ij} \sigma_{kk} = \sigma_{ij} - 1/3 \delta_{ij} (\sigma_{xx} + \sigma_{yy} + \sigma_{zz}) = \sigma_{ij} - \delta_{ij} P, \qquad (15)$$

where δ_{ij} is the Kronecker delta for which $\delta_{ij} = 1$ when $i = j$ and $\delta_{ij} = 0$ when $i \neq j$. Then, since $\sigma'_{xx} + \sigma'_{yy} + \sigma'_{zz} = 0$ from equation (15) and $\sigma'_{yy} / \sigma'_{xx} = \dot{\varepsilon}_{yy} / \dot{\varepsilon}_{xx}$ from equation (14),

$$\begin{aligned} \sigma_T &= \sigma_{xx} - \sigma_{zz} = (\sigma'_{xx} + P) - (\sigma'_{zz} + P) = \sigma'_{xx} - \sigma'_{zz} \\ &= \sigma'_{xx} + (\sigma'_{xx} + \sigma'_{yy}) = 2\sigma'_{xx} + \sigma'_{yy} = \left(2 + \sigma'_{yy} / \sigma'_{xx} \right) \sigma'_{xx} \\ &= \left(2 + \dot{\varepsilon}_{yy} / \dot{\varepsilon}_{xx} \right) \sigma'_{xx}. \end{aligned} \qquad (16)$$

The expression for σ_e uses $\sigma'_{ij} = \sigma'_{ji}$ because stress is a symmetrical tensor and uses $\sigma'_{ij} / \sigma'_{xx} = \dot{\varepsilon}_{ij} / \dot{\varepsilon}_{xx}$ by equation (14),

$$\begin{aligned} \sigma_e &= \left(1/2 \sigma'_{ij} \sigma'_{ji} \right)^{1/2} \\ &= \left[1/2 \left(\sigma'^2_{xx} + \sigma'^2_{yy} + \sigma'^2_{zz} + 2\sigma^2_{xy} + 2\sigma^2_{yz} + 2\sigma^2_{zx} \right) \right]^{1/2} \\ &= \left[\frac{1}{2} + \frac{1}{2} \left(\frac{\dot{\varepsilon}_{yy}}{\dot{\varepsilon}_{xx}} \right)^2 + \frac{1}{2} \left(\frac{\dot{\varepsilon}_{zz}}{\dot{\varepsilon}_{xx}} \right)^2 + \left(\frac{\dot{\varepsilon}_{xy}}{\dot{\varepsilon}_{xx}} \right)^2 + \left(\frac{\dot{\varepsilon}_{yz}}{\dot{\varepsilon}_{xx}} \right)^2 + \left(\frac{\dot{\varepsilon}_{zx}}{\dot{\varepsilon}_{xx}} \right)^2 \right]^{1/2} \sigma'_{xx} \end{aligned} \qquad (17)$$

Combining equations (14) and (17) for $\dot{\varepsilon}_{ij} = \dot{\varepsilon}_{xx}$,

$$\begin{aligned} \dot{\varepsilon}_{xx} &= \left[\frac{1}{2} + \frac{1}{2} \left(\frac{\dot{\varepsilon}_{yy}}{\dot{\varepsilon}_{xx}} \right)^2 + \frac{1}{2} \left(\frac{\dot{\varepsilon}_{zz}}{\dot{\varepsilon}_{xx}} \right)^2 + \left(\frac{\dot{\varepsilon}_{xy}}{\dot{\varepsilon}_{xx}} \right)^2 + \left(\frac{\dot{\varepsilon}_{yz}}{\dot{\varepsilon}_{xx}} \right)^2 + \left(\frac{\dot{\varepsilon}_{zx}}{\dot{\varepsilon}_{xx}} \right)^2 \right]^{\frac{n-1}{2}} \\ &\cdot \left(\frac{\sigma'_{xx}}{A} \right)^n = R (\sigma'_{xx} / A)^n, \end{aligned} \qquad (18)$$

where R is a scalar that captures the invariant property of σ_e. For linear creep along x, $\dot{\varepsilon}_{xx} = -\dot{\varepsilon}_{zz}$ and $\dot{\varepsilon}_{yy} = \dot{\varepsilon}_{xy} = \dot{\varepsilon}_{yz} = \dot{\varepsilon}_{zx} = 0$, so that $\sigma_T = 2\sigma'_{xx}$ in equation (16) and $R = 1$ in equation (18).

5. Creep of a Partly Grounded Ice Shelf

[18] The spreading rate for floating ice is obtained by using the flow law given by equation (18) to link strain rate $\dot{\varepsilon}_{xx}$ in equation (7) for the mass balance to tensile stress σ_T given by equations (13), (16), and (18) for the force balance,

$$\dot{\varepsilon}_{xx} = R \left(\frac{\sigma'_{xx}}{A} \right)^n = R \left[\frac{\rho_I g h_I}{2 (2 + \dot{\varepsilon}_{yy} / \dot{\varepsilon}_{xx}) A} \left(1 - \frac{\rho_I}{\rho_W} \right) \right]^n. \qquad (19)$$

Equation (19) gives the *Weertman* [1957a] strain rate for a freely floating ice shelf. For linear flow of buoyant ice, $\dot{\varepsilon}_{yy} = 0$, $R = 1$, and equations (7) and (19) give

$$\frac{dh_I}{dt} = a - h_I \dot{\varepsilon}_{xx} = a - h_I \left[\frac{\rho_I g h_I}{4A} \left(1 - \frac{\rho_I}{\rho_W} \right) \right]^n. \qquad (20)$$

[19] An ice shelf grounded at one end cannot thin uniformly because ice crossing the grounding line has a thickness gradient and velocity that differs from the creep thinning rate $\dot{\varepsilon}_{zz}$ of floating ice. Figure 2 shows an ice shelf of length L that calves at $x = 0$, where ice thickness h_I is specified as h_0 and inland ice reaches the calving front at negative velocity u_0. The equilibrium ice thickness gradient for floating ice is given by equation (6) with $\dot{\varepsilon}_{xx}$ given by equation (19) when $\dot{\varepsilon}_{yy} = 0$ and $R = 1$ for linear flow,

$$\frac{dh_I}{dx} = \frac{a h_I}{ax + h_0 u_0} - \frac{h_I^2}{ax + h_0 u_0} \left[\frac{\rho_I g h_I}{4A} \left(1 - \frac{\rho_I}{\rho_W} \right) \right]^n. \qquad (21)$$

Equation (21) was originally derived by *Van der Veen* [1983], who took h_0, u_0, and $x = 0$ at the ice-shelf grounding line with x positive downslope, so that u_0 is positive.

[20] To prevent lateral spreading, the ice shelf must be grounded along its sides and have constant width w_I. The compressive force F_C provided by lateral drag is

$$F_C = \sigma_C A_x = \sigma_C w_I h_I = \bar{\tau}_S A_y = 2\bar{\tau}_S \bar{h}_I x, \qquad (22)$$

where σ_C is a longitudinal compressive stress acting on transverse area $A_x = w_I h_I$ for ice thickness h_I at distance x from the calving front and $\bar{\tau}_S$ is an average side shear stress acting on side areas $A_y = 2\bar{h}_I x$ having average ice thickness $\bar{h}_I$ along distance x, so that

$$\sigma_C = \frac{2\bar{\tau}_S \bar{h}_I x}{w_I h_I} = \frac{2\bar{\tau}_S}{w_I h_I} \int_0^x h_I dx. \qquad (23)$$
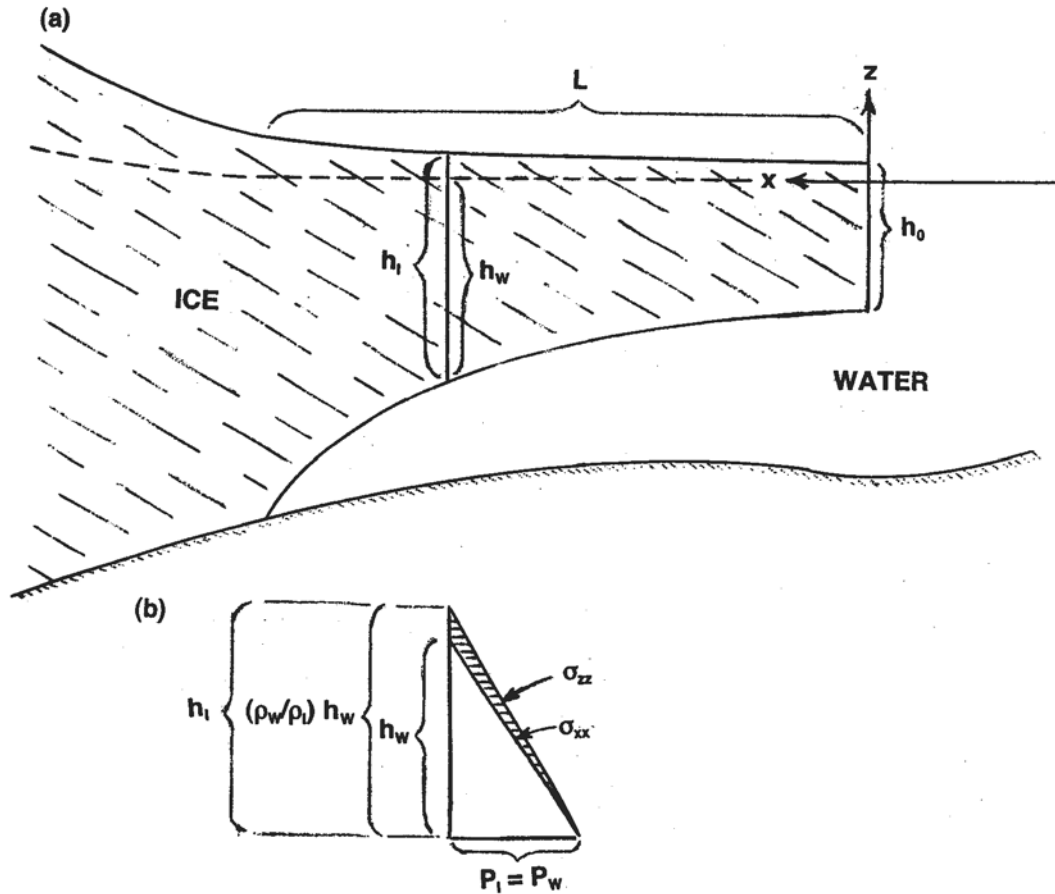
Figure 2. A geometrical representation of gravitational forcing for an ice shelf that thins seaward of its grounding line. (a) The concave ice thickness profile for shelf flow. (b) The gravitational driving force per unit width of ice is the shaded area between the increase with depth of compressive stresses σ_{zz} and σ_{xx} in floating ice.

Tensile stress σ_T in equation (13) is then replaced by $\sigma_T + \sigma_C$, so that

$$\sigma_T = 1/2\rho_I g h_I (1 - \rho_I/\rho_W) - \sigma_C. \tag{24}$$

Equation (19) with $2\sigma'_{xx} = \sigma_T + \sigma_C$ then gives the *Thomas* [1973a, 1973b] strain rate for a linear ice shelf buttressed along its sides (as in a fjord),

$$\dot{\varepsilon}_{xx} = \left[\frac{\rho_I g h_I}{4A}\left(1 - \frac{\rho_I}{\rho_W}\right) - \frac{\sigma_C}{2A}\right]^n. \tag{25}$$

Equation (25) applies for plane strain in which width w_I is constant for a linear ice shelf grounded at the back and sides, so that along the centerline $\dot{\varepsilon}_{yy} = \dot{\varepsilon}_{xy} = \dot{\varepsilon}_{yz} = \dot{\varepsilon}_{zx} = 0$ and $\dot{\varepsilon}_{xx} = -\dot{\varepsilon}_{zz}$ gives $R = 1$ in equation (18).

6. Creep of a Partly Buoyant Ice Stream

[21] Assume that stream flow begins as sheet flow for which $P_W/P_I \rightarrow 0$ and ends as shelf flow for which $P_W/P_I \rightarrow 1$. Then basal buoyancy must be included in the horizontal force balance along the ice stream. Let equation (4) give the ice thickness gradient, with x positive upslope from the ice-shelf calving front, where $x = 0$, $h_I = h_0$, and $u_x = u_0$ is the negative ice velocity, as shown in Figure 3. The horizontal

force balance is calculated for the vertical cross-section at distance x upstream from the calving front.

[22] The shaded area of the force triangle in Figure 3 gives the horizontal force $(\sigma_T + \sigma_C)w_I h_I$ caused when σ_{xx} is less compressive than σ_{zz} and causes longitudinal extending strain rate $\dot{\varepsilon}_{xx}$ because P_W/P_I increases downslope. If P_W/P_I decreases downslope, $\sigma_T + \sigma_C$ is negative because σ_{xx} is more compressive than σ_{zz} and $\dot{\varepsilon}_{xx}$ is negative for compressive flow. This can happen if an ice stream moves faster upslope than downslope, such as Kamb Ice Stream (formerly Ice Stream C) in Antarctica [*Joughin et al.*, 2002]. Basal buoyancy makes no contribution to ice flow when $h_W = 0$, so that $P_W/P_I = 0$ in equation (10c), $\sigma_{xx} = \sigma_{zz}$, $\dot{\varepsilon}_{xx} = 0$ and the area of the force triangle in Figure 3b is $1/2P_I h_I = 1/2\rho_I g h_I^2$ using equation (10a). When $\sigma_{xx} < \sigma_{zz}$, that area is reduced by the areas of triangle 1, rectangle 2, and triangle 3, to give the shaded area in Figure 3b. These areas are $1/2(P_I - P_W)[h_I - (\rho_W/\rho_I)h_W]$ for triangle 1, $(P_I - P_W)(\rho_W/\rho_I)h_W$ for rectangle 2, and $1/2P_W h_W$ for triangle 3. Equating the shaded area to $(\sigma_T + \sigma_C)h_I$ gives the geometrical force balance because it uses these geometrical representations of force. Triangle 1 is the force per unit width in ice not supported by basal water pressure P_W, and rectangle 2 shows that σ_{zz} at the base of triangle 1 is transmitted totally to the bed. Triangle 3
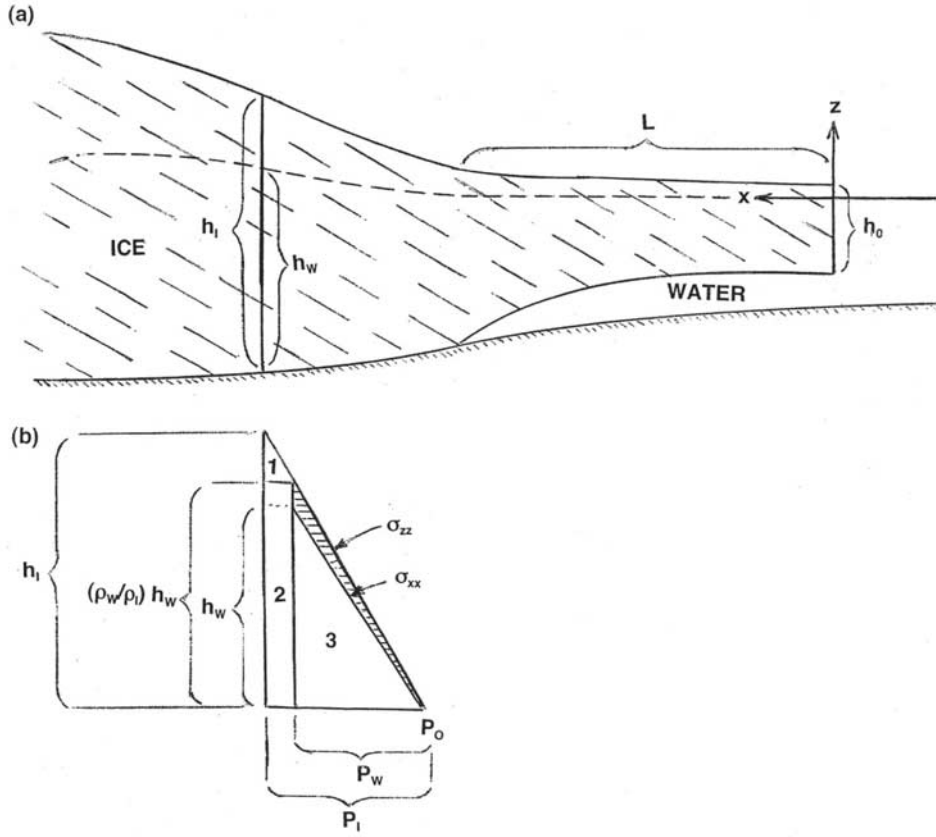
Figure 3. A geometrical representation of gravitational forcing for an ice stream that thins downstream and supplies ice to an ice shelf. (a) The concave ice thickness profile for stream flow that becomes shelf flow. (b) The gravitational driving force per unit width of ice is the shaded area between the increase with depth of compressive stresses σ_{zz} and σ_{xx} in ice that is supported both by basal water and the bed.

is the force per unit width that is supported totally by basal water pressure P_W. The horizontal force balance is then

$$1/2P_I h_I - 1/2(P_I - P_W)[h_I - (\rho_W/\rho_I)h_W] - (P_I - P_W)$$
$$\cdot (\rho_W/\rho_I)h_W - 1/2P_W h_W - (\sigma_T + \sigma_C)h_I = 0, \qquad (26)$$

where $1/2P_I h_I$ is the total area of triangle 1, rectangle 2, triangle 3, and the shaded area. Using equations (10) and solving for σ_T,

$$\sigma_T = 1/2P_I - 1/2(P_I - P_W)(1 - P_W/P_I) - (P_I - P_W)(P_W/P_I)$$
$$- 1/2P_W(\rho_I/\rho_W)(P_W/P_I) - \sigma_C$$
$$= 1/2P_I(1 - \rho_I/\rho_W)(P_W/P_I)^2 - \sigma_C$$
$$= 1/2\rho_I g h_I(1 - \rho_I/\rho_W)(P_W/P_I)^2 - \sigma_C. \qquad (27)$$

[23] Setting $\sigma_T = 2\sigma'_{xx}$ for linear stream flow in plane strain, as represented by Figure 3 for $\dot{\varepsilon}_{yy} = 0$ and $R = 1$, equation (27) can be substituted for σ'_{xx} in equation (18), which then gives $\dot{\varepsilon}_{xx}$ for the mass balance. Then the ice thickness gradient of stream flow is given by equation (6) for mass balance equilibrium,

$$\frac{dh_I}{dx} = \frac{h_I a}{ax + h_0 u_0} - \frac{h_I^2}{ax + h_0 u_0} \cdot \left[\frac{\rho_I g h_I}{4A}\left(1 - \frac{\rho_I}{\rho_W}\right)\left(\frac{P_W}{P_I}\right)^2 - \frac{\sigma_C}{2A}\right]^n.$$
$$(28)$$

Taking h_R as bedrock height above (positive) or depth below (negative) sea level, so $h = h_I + h_R$ is ice height above sea level, ice surface slope $\Delta h/\Delta x = \Delta h_I/\Delta x + \Delta h_R/\Delta x$ is

$$\frac{\Delta h}{\Delta x} = \frac{h_I a}{ax + h_0 u_0} - \frac{h_I^2}{ax + h_0 u_0}\left[\frac{\rho_I g h_I}{4A}\left(1 - \frac{\rho_I}{\rho_W}\right)\left(\frac{P_W}{P_I}\right)^2 - \frac{\sigma_C}{2A}\right]^n$$
$$+ \frac{\Delta h_R}{\Delta x}. \qquad (29)$$

[24] Note that equation (28) for stream flow reduces to equation (21) for linear shelf flow when $P_W/P_I = 1$ and $\sigma_C = 0$. Compressive stress σ_C arises from side shear stress τ_S averaged over distance x from the calving front of the ice shelf and basal shear stress τ_O averaged over distance $x - L$ from the ice-shelf grounding line. Compressive force F_C is

$$F_C = \sigma_C A_x = \bar{\tau}_S A_y + \bar{\tau}_O A_z = \sigma_C w_I h_I = 2\bar{\tau}_S \bar{h}_I x + \bar{\tau}_O \bar{w}_I(x - L),$$
$$(30)$$

where $A_x = w_I h_I$ is the transverse cross-sectional area at distance x upslope from the calving front, $A_y = 2\bar{h}_I x$ is the side area for average ice thickness $\bar{h}_I$ from x to the ice-shelf
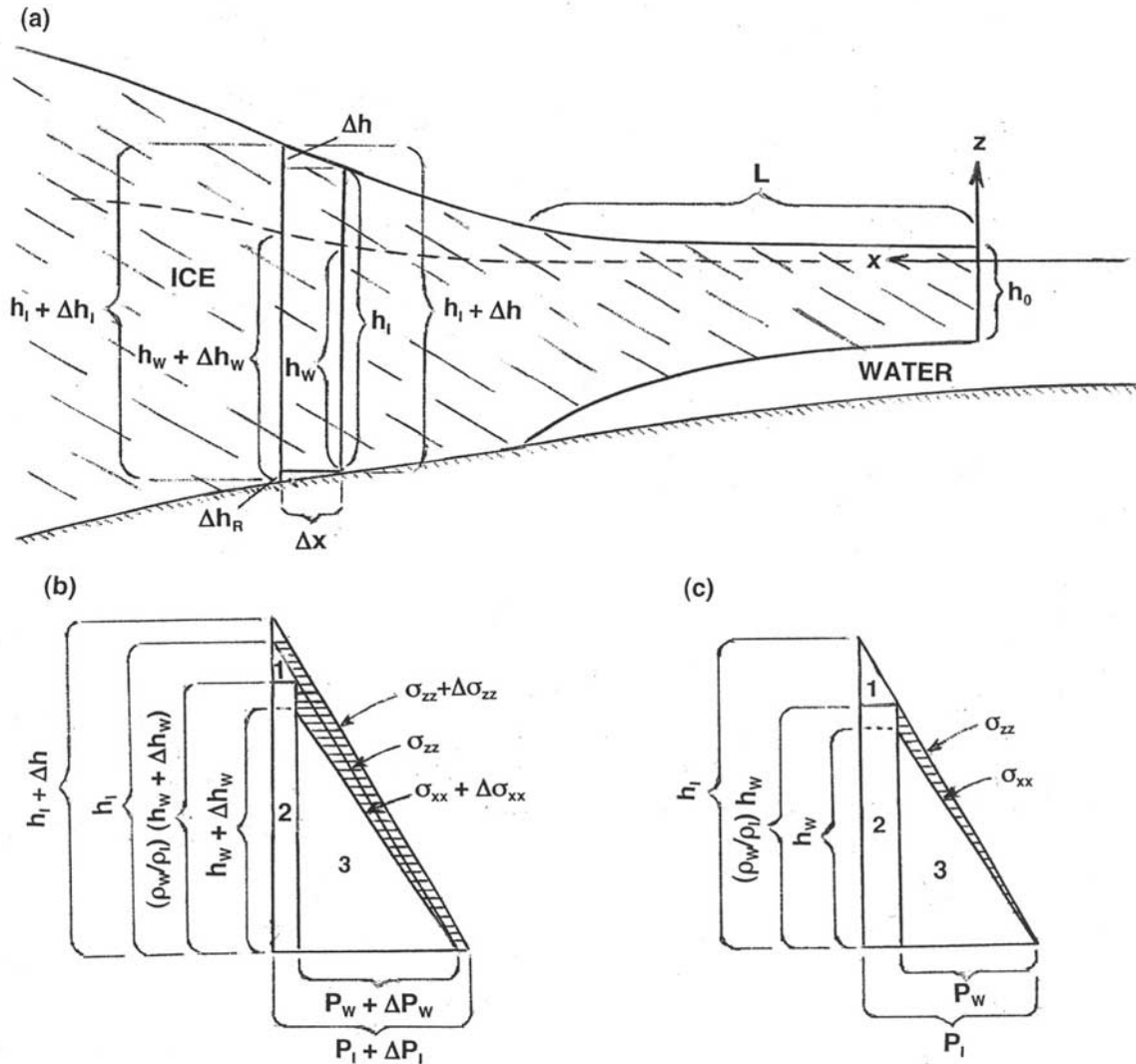
Figure 4. A geometrical representation of gravitational forcing showing an incremental addition to forcing for an ice stream that thins downstream and supplies ice to an ice shelf. (a) The concave ice thickness profile for stream flow that becomes shelf flow. Gravitational driving forces are applied to the vertical ice column. Ice thickness gradient $\Delta h_I/\Delta x$ contributes to gravitational forcing only through surface slope $\Delta h/\Delta x = \Delta h_I/\Delta x - \Delta h_R/\Delta x$. (b) The gravitational driving force per unit width of ice on the upstream side of the ice column is the shaded area between the increase with depth of compressive stresses $\sigma_{zz} + \Delta\sigma_{zz}$ and $\sigma_{xx} + \Delta\sigma_{xx}$ in distance Δx. Gravitational forcing is caused by surface slope $\Delta h/\Delta x$, basal buoyancy P_W/P_I, and gradient $\Delta(P_W/P_I)/\Delta x$ in basal buoyancy. (c) The gravitational driving force per unit width of ice on the downstream side of the ice column is the shaded area between the increase with depth of compressive stresses σ_{zz} and σ_{xx}. Ice is supported partly by the bed and partly by basal water along Δx, where $\Delta\sigma_{zz}$ makes σ_{zz} more negative (more compressive) and $\Delta\sigma_{xx}$ can make σ_{xx} more or less negative (compressive), but makes σ_{xx} more negative here. Gravitational forcing is caused by basal buoyancy P_W/P_I.

calving front, and $A_z = \bar{w}_I (x - L)$ is the basal area for an ice stream of average width $\bar{w}_I$. Solving for σ_C,

$$\sigma_C = \frac{2\bar{\tau}_S \bar{h}_I x}{w_I h_I} + \frac{\bar{\tau}_O \bar{w}_I (x - L)}{w_I h_I} = \frac{2\bar{\tau}_S}{w_I h_I} \int_0^x h_I dx + \frac{\bar{\tau}_O \bar{w}_I (x - L)}{w_I h_I}.$$

(31)

Since τ_S, τ_0, and h_I change continuously along x, it would be useful if these contributions to σ_C could be incorporated into equation (28) for $\Delta h_I/\Delta x$ at successive steps of incremental length Δx, width w_I, and height h_I above the bed where the ice column touches the bed at distance x upstream from the ice-shelf calving front and basal water pressure P_W would support water of height h_W above the bed, as seen in Figure 4a. At incremental distance Δx upstream, these heights would be $h_I + \Delta h_I$ and $h_W + \Delta h_W$, where Δh_I and Δh_W can be positive or negative. Ice elevation h above sea level increases by

Δh, so $\Delta h/\Delta x$ is the ice surface slope in incremental distance Δx.

[25] The horizontal force balance on the ice column in Figure 4 duplicates the forces in Figure 3 and over incremental length Δx adds side shear force $F_S = 2\tau_S(h_I + 1/2\Delta h_I)\Delta x$, basal shear force $F_O = \tau_O w_I \Delta x$, and positive or negative increment $\Delta\sigma_T$ to the tensile force F_T so that σ_T at x becomes $\sigma_T + \Delta\sigma_T$ at $x + \Delta x$ due to positive or negative change Δh_W in h_W. In the geometrical force balance, horizontal force per unit width $(\sigma_T + \Delta\sigma_T)(h_I + \Delta h_I)$ at $x + \Delta x$ offsets the shaded area in Figure 4b. This shaded area on the upslope side of the ice column is area $1/2(P_I + \Delta P_I)(h_I + \Delta h)$ minus the combined areas of triangle 1, rectangle 2, and triangle 3. The geometrical force balance for the horizontal direction is then

$$
\begin{aligned}
1/2(P_I + \Delta P_I)(h_I + \Delta h) &- 1/2(P_I - P_W)[h_I - (\rho_W/\rho_I)h_W] \\
&- (P_I - P_W)(\rho_W/\rho_I)h_W - 1/2P_W h_W \\
&- (\sigma_T + \Delta\sigma_T)(h_I + \Delta h_I) - \sigma_C h_I \\
&- 2\tau_S(h_I + 1/2\Delta h_I)\Delta x/w_I - \tau_O\Delta x \\
&= 0.
\end{aligned} \tag{32}
$$

Note that the first left-hand term in equation (32) is the gravitational term that depends on ice elevation change Δh, not on ice thickness change Δh_I. It is possible for Δh_I to result only from bed elevation change Δh_R, so that $\Delta h_I = \Delta h_R$ and $\Delta h = 0$. In this case there is no gravitational forcing due to surface slope because $\Delta h/\Delta x = 0$ [Hughes, 1998, pp. 144–145], but there is still gravitational forcing due to basal buoyancy, as represented by P_W/P_I. Ice thickness h_I is important because deviatoric stresses $\sigma_T + \Delta\sigma_T$ and τ_S act on respective areas $w_I (h_I + \Delta h_I)$ and $2 (h_I + 1/2\Delta h_I)\Delta x$ to give forces that resist the gravitational force. Compare Figure 4a with Figure 4b to see this distinction. The gravitational force represented geometrically by the shaded area in Figure 4b is applied in Figure 4a to an ice column that has a sloping top surface and a flat horizontal bottom surface, so that surface slope $\Delta h/\Delta x$ enters into the gravitational terms of the force balance but bed slope $\Delta h_R/\Delta x$ and ice thickness gradient $\Delta h_I/\Delta x$ do not. However, ice thickness gradient $\Delta h_I/\Delta x$ does enter into the resisting terms of the force balance and into the mass balance.

[26] Second-order terms containing $\Delta P_I \Delta h$, $\Delta\sigma_T \Delta h_I$, and $\Delta h_I \Delta x$ can be ignored in equation (32). For example $1/2\Delta P_I \Delta h$ is the area of the small unshaded and unnumbered triangle at the top of the geometrical representation of forces in Figure 4b, and it vanishes as Δx shrinks to zero, even though $\Delta h/\Delta x$ remains a finite surface slope. Making these simplifications and solving equation (32) for the first term using $P_I + \Delta P_I = \rho_I g(h_I + \Delta h)$ and using equation (10c) to introduce P_W/P_I,

$$
\begin{aligned}
1/2\rho_I g(h_I + \Delta h)(h_I + \Delta h) &= 1/2(P_I - P_W)(h_I - h_I P_W/P_I) \\
&+ (P_I - P_W)h_I P_W/P_I \\
&+ 1/2P_W h_I(\rho_I/\rho_W)(P_W/P_I) \\
&+ \sigma_T h_I \\
&+ \sigma_T \Delta h_I + h_I \Delta\sigma_T + \sigma_C h_I \\
&+ 2\tau_S h_I \Delta x/w_I + \tau_O\Delta x.
\end{aligned} \tag{33}
$$

Ignoring the term containing Δh^2, setting $h_I P_I = \rho_I g h_I^2$ from equation (10a), dividing by Δx, and solving for $\rho_I g h_I \Delta h/\Delta x$:

$$
\begin{aligned}
\rho_I g h_I \Delta h/\Delta x &= \left[-1/2 h_I P_W^2/P_I + h_I P_W - h_I P_W^2/P_I\right]/\Delta x \\
&+ \left[1/2 h_I(\rho_I/\rho_W)P_W^2/P_I + \sigma_T h_I + \sigma_T \Delta h_I \right. \\
&\quad \left. + h_I\Delta\sigma_T + \sigma_C h_I\right]/\Delta x + 2\tau_S h_I/w_I + \tau_O \\
&= \left[-1/2 h_I(1 - \rho_I/\rho_W)\left(P_W^2/P_I\right) + h_I(\sigma_T + \sigma_C)\right] \\
&\quad /\Delta x + \sigma_T\Delta h_I/\Delta x + h_I\Delta\sigma_T/\Delta x + 2\tau_S h_I/w_I + \tau_O.
\end{aligned} \tag{34}
$$

To keep the first right-hand term from becoming infinite as Δx shrinks to zero, it is necessary that, using equation (10a),

$$
\begin{aligned}
\sigma_T &= 1/2(1 - \rho_I/\rho_W)\left(P_W^2/P_I\right) - \sigma_C \\
&= 1/2\rho_I g h_I(1 - \rho_I/\rho_W)(P_W/P_I)^2 - \sigma_C.
\end{aligned} \tag{35}
$$

Then equation (34) becomes

$$
\begin{aligned}
\rho_I g h_I \Delta h/\Delta x &= \sigma_T\Delta h_I/\Delta x + h_I\Delta\sigma_T/\Delta x + 2\tau_S h_I/w_I + \tau_O \\
&= \Delta(\sigma_T h_I)/\Delta x + 2(h_I/w_I)\tau_S + \tau_O.
\end{aligned} \tag{36}
$$

The expression for σ_T given by equation (35) includes the contribution to σ_T from ice thickness h_I and basal buoyancy, represented by P_W/P_I, such that $\sigma_T + \sigma_C = 0$ when $P_W/P_I = 0$. Longitudinal extension of ice on a frozen bed, where $P_W/P_I = 0$, is assumed to be much smaller than extension when $P_W/P_I > 0$ for ice sliding on a thawed bed, so σ_T can be ignored when P_W/P_I is insignificant. This is an assumption that is reasonable for ice streams, but not at ice divides [Weertman, 1973]. Equation (36) is obtained from the force balance when P_W/P_I is ignored; for example, see Van der Veen's [1999] equation (3.3.12), in which $R_{xx} = \sigma_T$ and $R_{xy} = \tau_S$ at $y = w_I/2$).

[27] When P_W/P_I cannot be ignored because it causes σ_T, equation (35) can be differentiated to give the longitudinal gradient $\Delta\sigma_T/\Delta x$, where $\bar{h}_I = h_I + 1/2\Delta h_I$ and $\bar{w}_I = w_I + 1/2\Delta w_I$ in distance Δx and $\Delta w_I = 0$ for plane strain,

$$
\begin{aligned}
\frac{\Delta\sigma_T}{\Delta x} &= \frac{\rho_I g}{2}\left(1 - \frac{\rho_I}{\rho_W}\right)\left[\left(\frac{P_W}{P_I}\right)^2\frac{\Delta h_I}{\Delta x} + h_I\frac{\Delta(P_W/P_I)^2}{\Delta x}\right] \\
&- \frac{\Delta\sigma_C}{\Delta x} = \frac{\rho_I g}{2}\left(1 - \frac{\rho_I}{\rho_W}\right)\left[\left(\frac{P_W}{P_I}\right)^2\frac{\Delta h_I}{\Delta x} + h_I\frac{\Delta(P_W/P_I)^2}{\Delta x}\right] \\
&- \frac{2\bar{h}_I\Delta x(\Delta\tau_S/\Delta x) + \bar{w}_I\Delta x(\Delta\tau_O/\Delta x)}{(w_I + \Delta w_I)(h_I + \Delta h_I)} \\
&= \frac{\rho_I g}{2}\left(1 - \frac{\rho_I}{\rho_W}\right)\left[\left(\frac{P_W}{P_I}\right)^2\frac{\Delta h_I}{\Delta x} + h_I\frac{\Delta(P_W/P_I)^2}{\Delta x}\right] \\
&- \left[\frac{2(\bar{h}_I/w_I)\Delta\tau_S + \Delta\tau_O}{h_I + \Delta h_I}\right].
\end{aligned} \tag{37}
$$

Substituting equation (37) for $\Delta\sigma_T/\Delta x$ in equation (36) and collecting terms containing $\Delta h_I/\Delta x$, where $\Delta\sigma_S$ and $\Delta\tau_O$

are small compared to τ_S and τ_O, respectively, and can be ignored,

$$\rho_I g h_I \Delta h / \Delta x = \left[\rho_I g h_I (1 - \rho_I/\rho_W)(P_W/P_I)^2 - \sigma_C \right] \Delta h_I / \Delta x$$
$$+ 1/2 \rho_I g h_I^2 (1 - \rho_I/\rho_W) \Delta (P_W/P_I)^2 / \Delta x$$
$$+ 2(h_I/w_I)\tau_S + \tau_O. \qquad (38)$$

Substituting equation (28) for $\Delta h_I/\Delta x$ into equation (38) and solving for surface slope $\Delta h/\Delta x$,

$$\frac{\Delta h}{\Delta x} = \left\{ \left(1 - \frac{\rho_I}{\rho_W} \right) \left(\frac{P_W}{P_I} \right)^2 - \sigma_C \right\} \left\{ \frac{h_I a}{ax + h_0 u_0} \right.$$
$$\left. - \frac{h_I^2}{ax + h_0 u_0} \left[\frac{\rho_I g h_I}{4A} \left(1 - \frac{\rho_I}{\rho_W} \right) \left(\frac{P_W}{P_I} \right)^2 - \frac{\sigma_C}{2A} \right]^n \right\}$$
$$+ \frac{h_I}{2} \left(1 - \frac{\rho_I}{\rho_W} \right) \frac{\Delta(P_W/P_I)^2}{\Delta x} + \frac{2\tau_S}{\rho_I g w_I} + \frac{\tau_O}{\rho_I g h_I}. \qquad (39)$$

[28] Equation (39) allows σ_C in equation (28) to be determined at each Δx step from values of τ_S, τ_O, h_I, and $\Delta(P_W/P_I)$ at these steps, so that σ_C is cumulative for all Δx steps along x. This is the holistic approach to ice sheet modeling. For an ice sheet on a frozen bed, $P_W/P_I = \sigma_C = \tau_S = 0$ and equation (39) reduces to [Nye, 1952]

$$\frac{\Delta h}{\Delta x} = \frac{\tau_O}{\rho_I g h_I}. \qquad (40)$$

For an unconfined linear ice shelf, $P_W/P_I = 1$, $\sigma_C = \tau_S = \tau_O = 0$ and $\Delta h/\Delta x = (1 - \rho_I/\rho_W) \Delta h_I/\Delta x$, so that equation (39) reduces to [Van der Veen, 1983],

$$\frac{\Delta h_I}{\Delta x} = \frac{h_I a}{ax + h_0 u_0} - \frac{h_I^2}{ax + h_0 u_0} \left[\frac{\rho_I g h_I}{4A} \left(1 - \frac{\rho_I}{\rho_W} \right) \right]^n. \qquad (41)$$

For a linear tabular iceberg, $\Delta h_I/\Delta x = 0$ and equation (41) reduces to [Weertman, 1957]

$$\frac{a}{h_I} = \left[\frac{\rho_I g h_I}{4A} \left(1 - \frac{\rho_I}{\rho_W} \right) \right]^n. \qquad (42)$$

[29] The ice-thinning rate for converging or diverging sheet flow, stream flow, and shelf flow is given by solving equation (4) for dh_I/dt numerically integrated upstream from the ice-shelf calving front, where $x = 0$ and w_0, h_0, and u_0 are specified (u_0 is negative ice velocity),

$$\frac{dh_I}{dt} = a - h_I \left(1 + \dot{\varepsilon}_{yy}/\dot{\varepsilon}_{xx} \right) \dot{\varepsilon}_{xx} - \left[\frac{w_0 h_0 u_0 + (a - d\bar{h}_I/dt)\bar{w}_I x}{h_I w_I} \right] \frac{dh_I}{dx}. \qquad (43)$$

In equation (43), $\dot{\varepsilon}_{yy}/\dot{\varepsilon}_{xx} = \Delta w_I \bar{u}_x / w_I \Delta u_x$ in incremental length Δx, $\dot{\varepsilon}_{xx}$ is approximated by equation (19) modified for stream flow as in equation (35), with σ_C given by equation (31),

$$\dot{\varepsilon}_{xx} = R \left[\frac{\rho_I g h_I}{2(2 + \dot{\varepsilon}_{yy}/\dot{\varepsilon}_{xx})A} \left(1 - \frac{\rho_I}{\rho_W} \right) \cdot \left(\frac{P_W}{P_I} \right)^2 - \frac{\sigma_C}{(2 + \dot{\varepsilon}_{yy}/\dot{\varepsilon}_{xx})A} \right]^n, \qquad (44)$$

and $\Delta h_I/\Delta x$ is approximated by equation (38) for mass balance equilibrium,

$$\frac{\Delta h_I}{\Delta x} = \frac{\rho_I g h_I \Delta h/\Delta x - 1/2 \rho_I g h_I^2 (1 - \rho_I/\rho_W)\Delta(P_W/P_I)^2/\Delta x - 2(h_I/w_I)\tau_S - \tau_O}{\rho_I g h_I (1 - \rho_I/\rho_W)(P_W/P_I)^2 - \sigma_C}. \qquad (45)$$

Equation (43) is solved iteratively, with $d\bar{h}_I/dt = 0$ in the first iteration and summed along x for successive Δx steps in subsequent iterations. Solutions of equation (43) require knowing $\dot{\varepsilon}_{xx}$ and $\dot{\varepsilon}_{yy}$ or calculating them from variations of u_x and w_I along x for an ice sheet flowband; see equation (5). Equation (45) is for stream flow, in which $0 < P_W/P_I < 1$. It reduces to the basal drag equation $\tau_O = \rho_I g h_I \Delta h/\Delta x$ when $P_W/P_I = \sigma_C = \tau_S = 0$ for frozen-bed sheet flow, and it reduces to the basal buoyancy equation $\Delta h/\Delta x = (1 - \rho_I/\rho_W)\Delta h_I/\Delta x$ when $P_W/P_I = 1$ and $\sigma_C = \tau_S = \tau_O = 0$ for free-floating shelf flow.

[30] Basal shear stress τ_O in equation (45) can be related to P_W/P_I if it is assumed that a downstream increase in P_W/P_I is linked to progressive drowning or burying of bedrock bumps by basal water or water-saturated basal till that cannot support a basal shear stress. In the *Hughes* [1998, pp. 105–106] extension from sheet flow to stream flow of the *Weertman* [1957b] theory of basal sliding, bedrock bumps shaped like cubes are replaced by bumps shaped like pyramids having average height Λ and average separation Λ'. Then ice melts under high pressure at the top of pyramids and ice creeps under high stress at the base of pyramids, with both processes giving equal but slower ice sliding rates at the same distance Λ_o below the peaks for pyramids of all sizes. The average separation between Λ_o for all pyramids is Λ_0', where Λ_0/Λ_0' is equivalent to the controlling bed roughness factor in the *Weertman* [1957b] theory for basal sliding in sheet flow. In stream flow, however, basal water or water-saturated till progressively drowns or buries bedrock pyramids in the downstream direction, so that Λ_0' increases and causes an effective reduction in Λ_0/Λ_0'. Stream flow develops from sheet flow with $P_W/P_I \approx 0$ and ends in shelf flow with $P_W/P_I \approx 1$. Depth λ_o of water or till at the bed leaves $\Lambda_o - \lambda_o$ as the undrowned or unburied pyramid height. Then $(\Lambda_0 - \lambda_0)/\Lambda_0' = (\Lambda_0/\Lambda_0')(1 - \lambda_0/\Lambda_0)$, which is represented by $(\Lambda_0/\Lambda_0')(1 - P_W/P_I)^c$, where c is an empirical constant. The *Weertman* [1957b] sliding law extended to embrace both sheet flow and stream flow would have the form

$$u_s = \left[\frac{\tau_O}{B_o \left(\Lambda_o/\Lambda_o' \right)^2 (1 - P_W/P_I)^{2c}} \right]^m = \left[\frac{\tau_O}{B(1 - P_W/P_I)^{2c}} \right]^m, \qquad (46)$$

where u_s is the basal sliding velocity, B_o is a basal sliding parameter, $B = B_o (\Lambda_0/\Lambda_0')^2$ incorporates bed roughness, and $m = (n + 1)/2$ is a viscoplastic parameter that incorporates n in the flow law of ice. Equation (46) gives u_s for sheet flow when $P_W/P_I \rightarrow 0$, gives u_s for streamflow when $0 < P_W/P_I < 1$, and is indeterminate for shelf flow because $\tau_O = 0$ when $P_W/P_I = 1$. The expression for τ_O in equation (45) that equation (46) gives is

$$\tau_O = B(1 - P_W/P_I)^{2c} u_s^{1/m}. \qquad (47)$$

Since u_s nearly equals surface ice velocity u_x for ice streams, measuring u_x, w_I, h_I, $\Delta h_I/\Delta x$, and $\Delta h/\Delta x$ allows P_W/P_I to be calculated along an ice stream from equations (45) for specified values of B, m, and τ_S. Values of τ_S range from 80 kPA to 250 kPA for Whillans Ice Stream [*Raymond et al.*, 2001]. Calculated values of P_W/P_I could then be compared to measured values in boreholes along the centerline of an ice stream. *Engelhardt and Kamb* [1997] could have done this for Whillans Ice Stream.

[31] Equation (46) can be related to an empirical sliding law [e.g., *Budd et al.*, 1979] as follows:

$$u_s = \left[\frac{P_I^{2c}\tau_O}{B(P_I - P_W)^{2c}}\right]^m = \frac{C\tau_O^m}{(P_I - P_W)^s}, \qquad (48)$$

provided that $C = P_I^s/B^m$ and $s = 2 \times c \times m$. However, basal sliding theory has not progressed to allow this level of precision. Empirically, $m \approx 3$ and $s \approx 1$, for which $c \approx 1/6$. Equation (46) has the advantage of relating P_W/P_I to water depth λ_o, which is calculated from the volume of basal water from place to place that is produced by the *Johnson* [2002] map-plane model of subglacial hydrology. His model then provides a physical basis for calculating P_W/P_I along ice streams, and P_W/P_I becomes the dynamic link for coupling models of ice sheets with models of subglacial hydrology [*Johnson and Fastook*, 2002].

7. Comparing the Analytical and Geometrical Force Balances

[32] In general, the dynamic components of an ice sheet are ice domes, ice streams, and ice shelves. Ice streams are the vehicles for concentrating sheet flow spreading from ice domes because they discharge up to 90% of ice from ice sheets into the sea, where an ice sheet becomes afloat as a calving ice shelf. The major variable for quantifying this transformation from fully grounded ice to fully floating ice is the basal buoyancy factor P_W/P_I, which in sheet flow is zero for a frozen bed or nearly zero for a thawed bed and in shelf flow is unity. In stream flow, P_W/P_I increase, usually irregularly, from nearly zero to unity from the head to the foot of the ice stream at the ice-shelf grounding line.

[33] The importance of P_W/P_I has been overlooked in glaciology because pioneering work on the force balance considered only a local balance of gravitational driving forces resisted by kinematic forces. All these forces act on an ice column, illustrated in Figure 1 for sheet flow, and lead to equation (40). The local force balance is in all the books [see *Hütter*, 1983; *Paterson*, 1994; *Hooke*, 1998; *Hughes*, 1998; *Van der Veen*, 1999]. Forces are balanced on a vertical column of ice whose gravitational motion is resisted by basal shear stress τ_O, side shear stress τ_S, and the gradient $\partial(h_I\sigma_T)/\partial x$ that includes longitudinal deviator stress σ_T; see equation (36). When modeling advance and retreat of ice sheets over time, it is customary to consider only τ_O as resisting gravitational forcing, with τ_O linked to ice thickness and ice surface slope; see equation (40). This procedure is a result of an analytical force balance that leads to the equilibrium equations (also called the momentum equations), which in tensor form can be written as

$$\partial\sigma_{ij}/\partial j + \rho_I g_i = 0. \qquad (49)$$

When x and y are horizontal and z is vertical upward in the ice column, for $i = z$ with $g_z = -g$,

$$\partial\sigma_{zx}/\partial x + \partial\sigma_{zy}/\partial y + \partial\sigma_{zz}/\partial z + \rho_I g_z = 0. \qquad (50)$$

Only the last two terms are important, so equation (50) can be integrated to give, for $z = 0$ at the base,

$$\sigma_{zz} = -\int_{\sigma_{zz}}^0 d\sigma_{zz} = \rho_I g_z \int_z^{h_I} dz = -\rho_I g(h_I - z). \qquad (51)$$

This gives the linear variation of σ_{zz} with z, shown for the geometrical force balance in Figures 1 through 4, but with $z = 0$ at the base of the ice, where $\sigma_{zz} = P_O = P_I$. When $i = x$,

$$\partial\left[2\sigma_{xx}' - \rho_I g(h_I - z)\right]/\partial x + \partial\sigma_{xy}/\partial y + \partial\sigma_{xz}/\partial z = 0, \qquad (52)$$

where $\sigma_{xx} = 2\sigma_{xx}' + \sigma_{zz}$ when $\dot{\varepsilon}_{yy} = 0$, as shown by equation (16). Ignoring σ_{zx}' and σ_{xy}, integrating equation (52) gives

$$\tau_O = -\int_{\tau_O}^O d\sigma_{xz} = -\rho_I g \int_0^{h_I} [\partial(h_I - z)/\partial x]dz$$

$$= -\rho_I g\alpha \int_0^{h_I} d(h_I - z) = \rho_I g h_I \alpha. \qquad (53)$$

This is identical to equation (40) obtained from the geometrical force balance for linear sheet flow, where $\alpha = \Delta h/\Delta x$ is the surface slope as $\Delta x \to 0$.

[34] Equation (52) can also be integrated for linear shelf flow along x, as shown by *Van der Veen* [1999, pp. 35–36, 128]. Integrating over z, noting that σ_{xx}' is constant through h_I and $\partial\sigma_{xy}/\partial y = \partial\sigma_{xz}/\partial z = 0$ for a linear ice shelf with $z = h$ at its surface and $z = h - h_I$ at its base,

$$\frac{\partial}{\partial x}\int_{h-h_I}^h 2\sigma_{xx}'dz = \frac{\partial}{\partial x}\int_{h-h_I}^h \rho_I g(h-z)dz = \rho_I g h_I \frac{dh}{dx} = \frac{\partial(2\sigma_{xx}'h_I)}{\partial x}. \qquad (54)$$

Substituting $h = (1 - \rho_I/\rho_W) h_I$ for full basal buoyancy ($P_W/P_I = 1$),

$$\rho_I g h_I(1 - \rho_I/\rho_W)dh_I/dx = 1/2\rho_I g(1 - \rho_I/\rho_W)d(h_I^2)/dx$$

$$= d(2\sigma_{xx}'h_I)/dx. \qquad (55)$$

[35] Multiplying by dx, integrating, and solving for σ_{xx}',

$$\sigma_{xx}' = 1/4\rho_I g h_I(1 - \rho_I/\rho_W), \qquad (56)$$

where the constant of integration is zero because $\sigma_{xx}' = 0$ when $h_I = 0$. Equation (56) is identical to equation (13) obtained from the geometrical force balance, since $\sigma_T = 2\sigma_{xx}'$ for a linear ice shelf.

[36] These integrations of the equilibrium equations demonstrate that no procedure exists for relating σ_{xx}' to P_W/P_I, as was done using the geometrical force balance to obtain equation (35), in which $\sigma_T = 2\sigma_{xx}'$ when $\dot{\varepsilon}_{yy} = 0$. Although P_W/P_I contributes to σ_{xx}' in the analytical force balance expressed by equation (52), the explicit relationship given by equation (27) when $\sigma_T = 2\sigma_{xx}'$ is provided only by the

geometrical force balance. The analytical force balance provides solutions only for $P_W/P_I = 0$ (linear sheet flow) and $P_W/P_I = 1$ (linear shelf flow). For these analytical solutions in the map-plane, see *Greve* [1997] for sheet flow and *Weis et al.* [1999] for shelf flow.

[37] To complete this comparison, it should be noted that ρ_I was assumed to be constant with depth in ice and bending at the ice-shelf calving front caused by the asymmetry of $\sigma_{xx} - \sigma_{zz}$ shown in Figure 1 was ignored. *Robin* [1958] shows how $\sigma_{xx} - \sigma_{zz}$ is affected by ice density that increases with depth due to compaction of snow, and *Reeh* [1968] shows how $\sigma_{xx} - \sigma_{zz}$ causes bending near the calving front. These features have no serious effect on the geometrical force balance. At some distance behind the calving front, $\sigma_{xx} - \sigma_{zz}$, and therefore $\dot{\varepsilon}_{xx}$, is constant through the ice thickness. It should also be noted that the geometrical force balance is coupled through longitudinal strain rate $\dot{\varepsilon}_{xx}$ to a mass balance to show that side shear and basal shear forces are cumulative upstream from the ice-shelf calving front. Therefore an ice column cannot be treated in isolation, as in the analytical force balance. Finally, basal buoyancy factor P_W/P_I is a statistical ratio over basal area $\bar{w}_I \Delta x$ in numerical integrations of equations (43) through (45). In this area, $P_W/P_I = 0$ where the bed is frozen, $P_W/P_I \rightarrow 0$ where the bed is only dampened when thawed, $P_W/P_I \rightarrow 1$ where basal water is able to drown most bedrock bumps or supersaturate basal till, and $P_W/P_I = 1$ when ice floats above the bed. Therefore P_W/P_I is a measure of the availability of basal water. It may be that values of P_W/P_I needed to fit the concave profiles of ice streams are statistical combinations of $P_W/P_I \approx 0$ and $P_W/P_I \approx 1$ along a given ice stream. Poor hydraulic conductivity between these patches is required to keep $0 < P_W/P_I < 1$ over area $\bar{w}_I \Delta x$ in a statistical sense. It is unclear how the distribution of P_W/P_I in space and time can be related to theories for subglacial hydrology, such as those developed by *Weertman* [1972], *Kamb* [2001], and *Johnson* [2002]. However, it seems reasonable that water under ice streams has tortuous flow paths from sites of basal melting where $P_W/P_I \rightarrow 1$ to sites of basal freezing where $P_W/P_I \rightarrow 0$, while avoiding sites where $P_W/P_I = 0$ because the bed is frozen.

8. Discussion and Conclusions

[38] The geometrical force balance has a major advantage over the analytical force balance because it includes basal buoyancy, represented by P_W/P_I, as well as surface slope $\Delta h/\Delta x$. Basal buoyancy allows a continuous transition from sheet flow to stream flow to shelf flow by allowing P_W/P_I to increase downslope from $P_W/P_I \approx 0$ to $P_W/P_I \approx 1$ along the length of an ice stream.

[39] The analytical force balance requires that for a given ice thickness, gravitational forcing depends only on the ice surface slope. In ice streams, however, the concave ice surface requires the surface slope to approach zero as ice velocity increases downstream. Concave ice stream surface profiles were originally generated simply by letting basal shear stress τ_O in equation (40) approach zero in the downstream direction [*Hughes*, 1981]. When the mass balance equation is applied to these concave longitudinal ice stream profiles, however, ice streams then acquire the property of a perpetual motion machine in which velocity

increases as gravitational forcing given by equation (40) decreases. This dilemma is avoided in a geometrical force balance because basal buoyancy replaces surface slope as the source of gravitational forcing in the downstream direction, and becomes dominant when the ice stream becomes a floating ice shelf. Basal buoyancy pushes ice up into the air above sea level, so that ice floating above water moves forward to displace air. An ice surface slope also allows ice to move forward and displace air in the downslope direction. Hence both basal buoyancy and surface slope allow forward gravitational motion.

[40] *Engelhardt and Kamb* [1997] report that P_W/P_I is close to unity near the head of Whillans Ice Stream (formerly Ice Stream B), such that basal water rises above sea level in boreholes to the bed, which means there is not perfect hydraulic conductivity to the sea. Basal water at this distance x from the ice front is being discharged downstream. Whether the seaward gradient of basal water pressure may fall to zero over time to establish hydraulic equilibrium is unknown. The derivation leading to equations (24) and (25), which then led to all subsequent equations containing the quantity $h_I(1 - \rho_I/\rho_W)$ for the height of ice floating above water, depends on perfect hydraulic conductivity between water under the ice and water in front of the ice, as illustrated in Figures 1 through 3.

[41] Terrestrial ice streams that end on land as ice lobes, such as those along the southern margin of the former Laurentide Ice Sheet at the Last Glacial Maximum, are not buttressed by water at their fronts. If basal buoyancy also provides gravitational forcing for those ice streams, then basal water generated beneath terrestrial ice streams must either freeze beneath the ice lobes to become regelation ice, or soak into an aquifer, or be discharged around the perimeter of the ice lobe, or some combination of these. For all of these scenarios, there is no "back force" from water pressure acting on ice below sea level at the ice front, as there is for floating ice shelves and, presumably, for ice streams that supply the ice shelves. Nonetheless, the geometrical force balance as derived here includes a "back force" of water pushing against floating ice, so that $h_I(1 - \rho_I/\rho_W) = 0.1\,h_I$ for $\rho_I = 900$ kg/m^3 and $\rho_W = 1000$ kg/m^3. For the geometrical force balance to apply to both marine and terrestrial ice streams, this quantity should be replaced by $h_I[1 - f_W(\rho_I/\rho_W)]$, where f_W is a water-buttressing fraction at the ice front where $x = 0$ that pushes against portion $h_I f_W(\rho_W/\rho_I)$ of buoyant ice thickness $h_I[1 - f_W(\rho_I/\rho_W)][P_W/P_I]^2$ at distance x upstream from the ice front. Then $f_W = 1$ when the ice front is fully floating and $f_W = 0$ when it is fully grounded. When basal water at distance x rises higher than the elevation of water at the ice front, as observed for some West Antarctic ice streams, then $0 < f_W < 1$ such that f_W satisfies the geometrical force balance. Figure 5 shows two Antarctic flowbands along which f_W probably varies. A cartoon showing how gravitational forcing is increased when $f_W < 1$ is shown in Figure 6 for a flowband from the West Antarctic ice divide to Pine Island Bay by way of Thwaites Glacier. Ice in this region is now thinning rapidly [*Zwally et al.*, 2002a].

[42] The holistic approach applies to all ice streams, whether they end as an ice shelf floating in water where $f_W = 1$, as an ice wall grounded in water where $0 < f_W < 1$, or
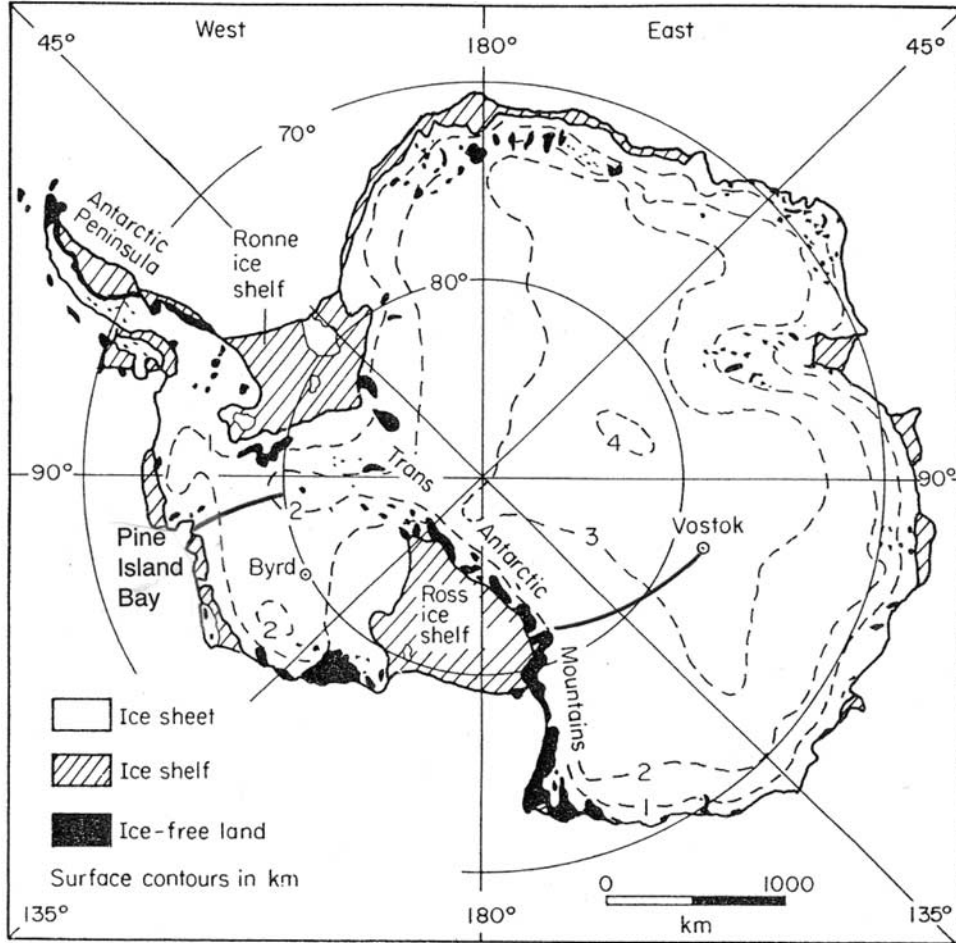
Figure 5. An Antarctic location map. The heavy lines show a West Antarctic flowband from the ice divide to Pine Island Bay by way of Thwaites Glacier, and an East Antarctic flowband from a subglacial lake at Vostok to the Ross Ice Shelf by way of Byrd Glacier.

as an ice lobe grounded on dry land where $f_W = 0$. Including f_W in equation (27) for σ_T, with σ_C given by equation (31) and $\rho_I h_I = \rho_W h_W$ for floating ice,

$$
\begin{aligned}
\sigma_T &= 1/2\rho_I g h_I [1 - f_W(\rho_I/\rho_W)][P_W/P_I]^2 - \sigma_C \\
&= 1/2\rho_I g h_I (P_W/P_I)^2 - 1/2\rho_I g h_I f_W(\rho_I/\rho_W)(P_W/P_I)^2 - \sigma_C \\
&= \frac{\rho_I g h_I}{2}\left(\frac{P_W}{P_I}\right)^2 - f_W\left(\frac{h_W}{h_I}\right)\left(\frac{\rho_W g h_W}{2}\right)\left(\frac{P_W}{P_I}\right)^2 - \frac{2\bar{\tau}_S \bar{h}_I x}{w_I h_I} \\
&\quad - \frac{\bar{\tau}_O(x - L)}{h_I}.
\end{aligned}
\tag{57}
$$

When multiplied by $w_I h_I$, equation (57) is the longitudinal force balance. Equation (57) highlights gravitational forcing in the first right-hand term resisted by water buttressing, side shear, and basal shear in the second, third, and fourth right-hand terms, respectively. Now consider a flowband on a frozen bed from a grounded ice margin where $f_W = L = 0$ to a subglacial lake where $P_W/P_I = 1$. Assume $\bar{\tau}_S = \tau_S = 0$ and $\bar{\tau}_0 = \tau_0$ is constant along x. Integrate equation (40) for a horizontal bed so that $h_I = h$ gives the parabolic flowband profile $x = (\rho_I g/2\tau_0)h_I^2$. Then equation (57) gives $\sigma_T = 0$ above the subglacial lake.

[43] Therefore, I maintain that gravitational forcing in ice streams has three components: surface slope $\Delta h/\Delta x$, basal buoyancy P_W/P_I, and water buttressing f_W, all represented geometrically in Figure 6. These components are not independent of each other. For example, suppose the terminal ice lobe of a terrestrial ice stream lies on a bed of ice-cemented permafrost that suddenly thaws and becomes slop that provides no basal traction for the overlying ice. The ice lobe will thin rapidly as $P_W/P_I = 0$ becomes $P_W/P_I = 1$, under the lobe. If basal meltwater creates a lake that floats the ice margin, then $f_W = 0$ becomes $f_W = 1$ over time. These changes in P_W/P_I and f_W cause surface slope $\Delta h/\Delta x$ to change all along the length of the ice stream. The holistic approach to ice sheet modeling is necessary in order to quantify how these three components of gravitational forcing interact with each other and with forces that resist gravitational motion along an ice stream. Basal water pressure increases locally to provide the gravitational forcing needed to overcome downstream resistance to ice flow when the ice lobe is frozen to its bed. This buildup in mountain glaciers leads to glacial surges when upslope ice-bed uncoupling due to high P_W/P_I propagates downslope to the terminus [*Kamb et al.*, 1985]; why not in ice streams, thereby allowing ice sheets to trigger rapid climate change?
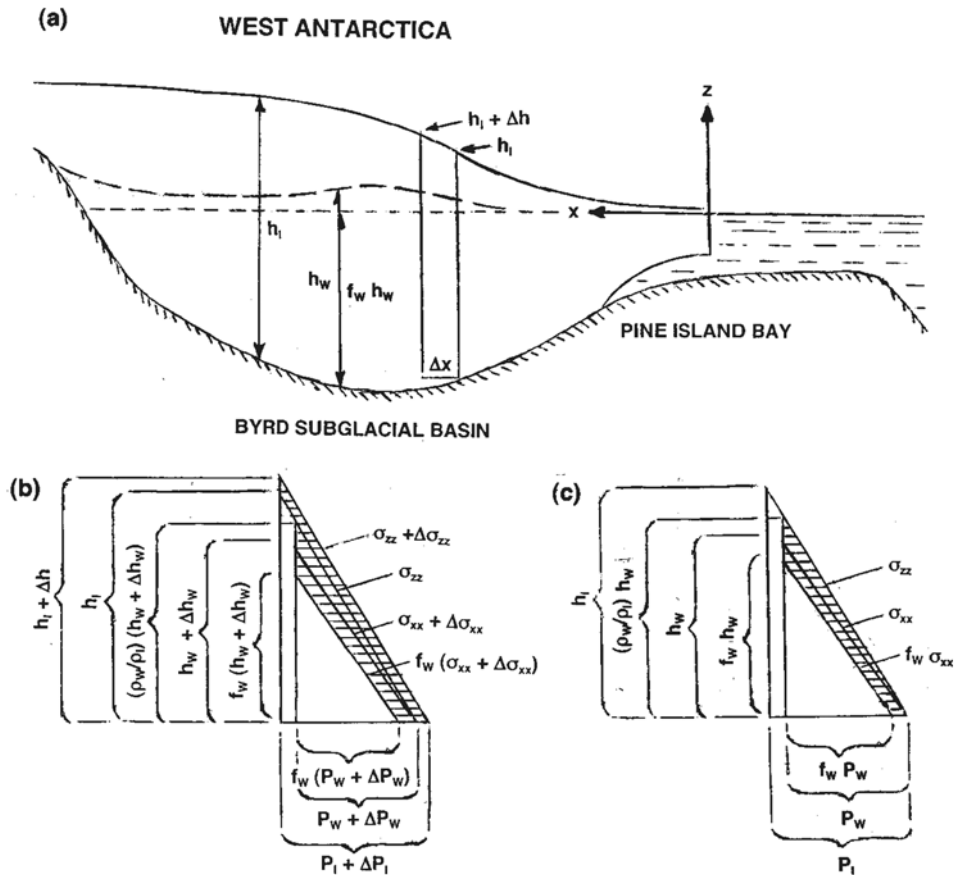
Figure 6. A cartoon showing how decreasing buttressing water fraction f_W can increase gravitational forcing along the West Antarctic flowband shown in Figure 5. (a) The flowband profile showing that $f_W = 1$ along the part of Thwaites Glacier floating in Pine Island Bay, and $0 < f_W < 1$ up the grounded part of Thwaites Glacier to the ice divide. (b) Reducing f_W increases the shaded area that geometrically represents the gravitational force per unit flowband width by adding the shaded strip between ($\sigma_{xx} + \Delta\sigma_{xx}$) and $f_W (\sigma_{xx} + \Delta\sigma_{xx})$ at flowband distance $x + \Delta x$ from the calving front. (c) Reducing f_W increases the shaded area by adding the shaded strip between σ_{xx} and $f_W\sigma_{xx}$ at flowband distance x from the calving front.

[44] A requirement of the geometrical force balance is that basal water will flow down the gradient $\Delta P_W/\Delta x$ in an ice stream. This gradient can be both outward toward the ice sheet margin and inward toward interior ice domes that are frozen to the bed, provided that the gradient causes h_W given by equation (10b) to decrease in both directions. Basal water flowing inward tends to pry the ice sheet loose from its bed, thereby hastening its gravitational collapse. This tendency has been proposed as the mechanism now driving gravitational collapse of the West Antarctic Ice Sheet into the Ross Sea embayment by ice stream surges [*Hughes*, 1975], a process having some observational support [*Bindschadler*, 1997]. It is opposed by outward flow of ice that acts like a rolling pin squeezing basal meltwater toward the ice sheet margin, especially along ice streams, and by freezing of basal meltwater as it comes in contact with colder interior ice.

[45] The concept of gravitational forcing by basal buoyancy, quantified by P_W/P_I, is inherent in the geometrical force balance. It provides a description of how ice streams behave and how they can destabilize an ice sheet, thereby

hastening gravitational collapse and rapid climate changes triggered by rapid collapse. Further investigation of this concept awaits a fuller understanding of subglacial hydrology. Progress toward this goal requires a map-plane model of subglacial hydrology, similar to the one developed by *Johnson* [2002] that can be coupled to a map-plane model for ice sheets [*Johnson and Fastook*, 2002]. The ice sheet model must generate ice streams by incorporating gravitational forcing due to basal buoyancy. No such ice sheet models exists at present. Both models should be holistic, so that processes near the ice sheet margin and beyond the margin, quantified by water buttressing f_W at the margin, affect flow of interior ice and water at the bed.

[46] As an incentive to accomplish this task, consider as a thought experiment the consequences of rejecting water buttressing f_W. Ice over subglacial Lake Vostok in central East Antarctica is 4 km thick [*Kwok et al.*, 2000], and $P_W/P_I = 1$. This ice moves very slowly because gravitational forcing arises from a tiny surface slope due to a small ice-thickness gradient. There is no gravitational forcing by basal buoyancy because ice is firmly grounded around the entire
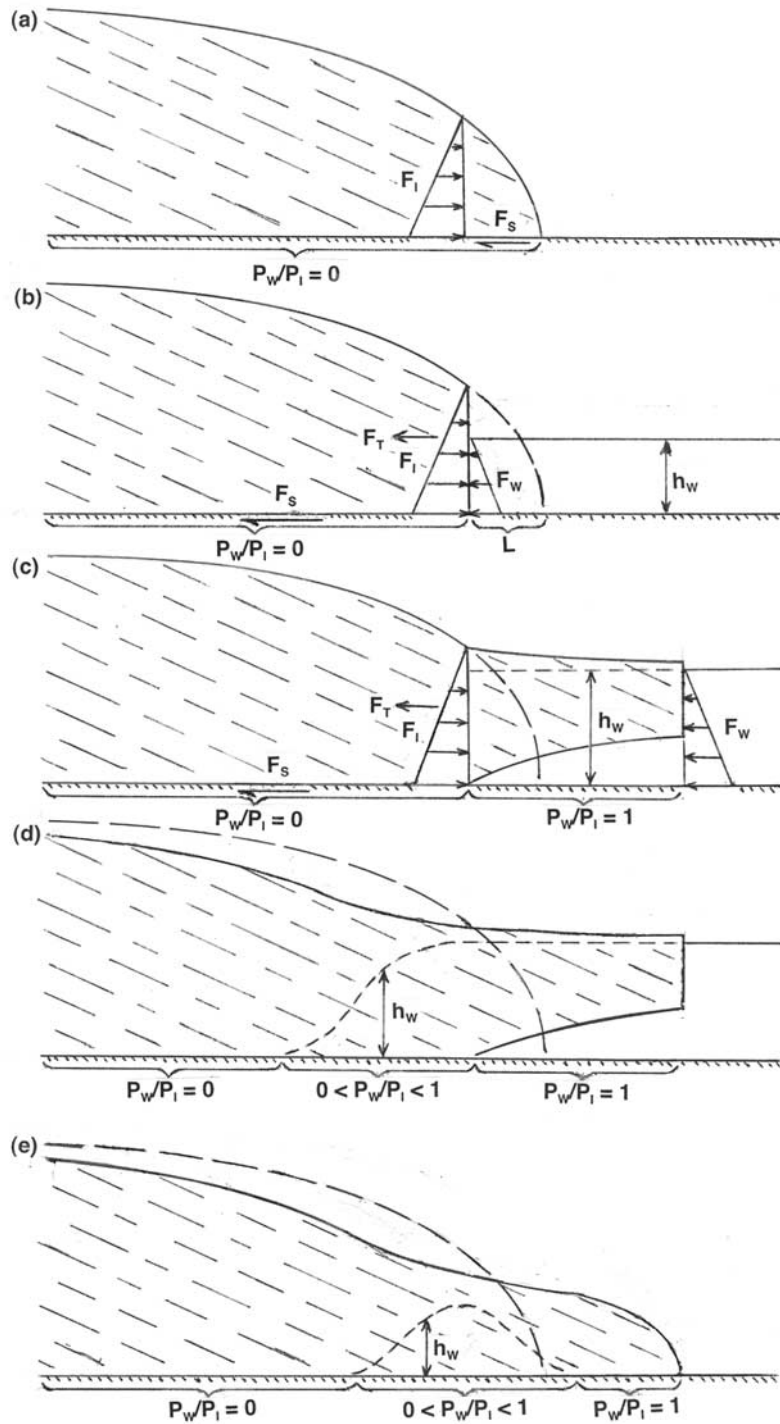
Figure 7.   A cartoon showing how basal buoyancy, defined as the ratio of basal water pressure P_W to ice overburden P_I, might trigger gravitational collapse of an ice sheet. (a) Gravitational force F_I in ice is balanced by shear force F_S on a frozen horizontal bed, where $P_W/P_I = 0$. (b) Water rising at the ice margin creates a calving ice wall that retreats distance L to where F_I is balanced by gravitational force F_W in water against the wall, tensile force F_T in ice behind the wall, and F_S in ice frozen to the bed. (c) Water rises high enough convert the calving ice wall into a floating ice shelf where $P_W/P_I = 1$, with ice at the grounding line still balanced by F_W at the calving front and by F_T and F_S behind the grounding line, where ice is still frozen to the bed. (d) Basal buoyancy propagates upslope from the grounding line, converting sheet flow into stream flow where $0 < P_W/P_I < 1$ at the bed, thereby lowering the ice surface in gravitational collapse. (e) Basal buoyancy propagates both upslope and downslope in the ablation zone of Figure 7a, where surface meltwater can reach the bed through crevasses, thereby lowering the ice surface in gravitational collapse upslope and extending the ice margin as an ice lobe downslope.

perimeter of the lake, so $\sigma_T = 0$ because $\sigma_C = 1/2\rho_I g h_I [1 - f_W (\rho_I/\rho_W)]$ in equation (57). Now imagine the lake was extended along the ice flowband that enters the Ross Ice Shelf through Byrd Glacier, as shown in Figure 5. Then σ_C would drop drastically, being caused only by $\bar{\tau}_S$ in equation (23), where $\tau_S \approx 250$ kPa seems to be an upper limit [*Raymond et al.*, 2001]. With $P_W/P_I = 1$ and $f_W = 1$ causing full flotation fully buttressed by water along this flowband, equation (54) gives $\sigma_T + \sigma_C = 1800$ kPa for ice above Lake Vostok. The "pulling power" due to basal buoyancy would be substantial. Just across the East Antarctic ice divide, such a lake may have found an outlet to the sea by draining into Lambert Glacier, with enormous downdraw of East Antarctic ice as a result [*Denton and Hughes*, 2002]. Now remove water buttressing at Lake Vostok, so that $f_W = 0$ removes the water buttressing term from equation (57). Then $\sigma_T + \sigma_C = 18{,}000$ kPa. The two results keep σ_T about the same only if σ_C increases ten-fold when $f_W = 1$ is replaced by $f_W = 0$. Otherwise σ_T will pull ice out much faster after f_W decreases.

[47] Now consider the flowband from Lake Vostok to Byrd Glacier, for which $x = 900$ km and $\bar{h}_I \approx 3$ km [*Drewry*, 1983]. Along the flowband, assume that $\bar{\tau}_S = 100$ kPa averaged from $\tau_s = 0$ at Lake Vostok to $\tau_s = 200$ kPa at Byrd Glacier [*Whillans et al.*, 1989], with $h_I = 4$ km and $w_I = 230$ km at Lake Vostok across the flowband to Byrd Glacier [*Kwok et al.*, 2000]. The longitudinal back force $\sigma_C w_I h_I$ at Lake Vostok is caused by side shear force $2\bar{\tau}_S\bar{h}_I x$ along the flowband, which gives $\sigma_C \approx 600$ kPa from equation (23). Equation (57) gives $\sigma_T + \sigma_C \approx 1800$ kPa when $f_W = 1$ and 18,000 kPa when $f_W = 0$. Then $\sigma_T \approx 1200$ kPa and $\sigma_T \approx 17{,}400$ kPa, respectively. A ten-fold increase in σ_C is not possible for floating ice, so catastrophic downdraw of ice by σ_T must take place unless basal grounding increases σ_C by including basal shear stress τ_O in the force balance.

[48] An ice stream 700 km long, grounded above sea level, and possibly uncoupled from the bed by meltwater originating from a subglacial volcano at the head of the ice stream, drains the northeast part of the Greenland Ice Sheet [*Fahnestock et al.*, 2001a, 2001b; *Day*, 2002]. It qualifies as a terrestrial ice stream, rather than a marine ice stream, because it is grounded above sea level except near its terminus. Taking $n = 3$ and setting $f_W = 0$ to remove the water buttressing term from equation (57), this ice stream would have an extending strain rate some three orders of magnitude greater than seen in a marine ice stream of comparable size. There is nothing in its dynamics, or in the glacial geological record for ice lobes of the former Laurentide Ice Sheet, to demonstrate that terrestrial ice streams without water buttressing in equation (57) have 1000 times the long-term extending strain rate because of a frictionless bed that is observed for marine ice streams grounded below sea level and buttressed by seawater, but also on a frictionless bed. *Clark* [1992, 1994, 1995] showed that southern Laurentide ice lobes were thin, hence ice-bed coupling was poor. Short-term catastrophic advance of ice lobes would be inevitable. Again, a definitive answer to this question will not emerge until ice sheet models that allow variations in both P_W/P_I and f_W are coupled to models of subglacial hydrology, both models being in the map plane. This requires holistic modeling.

[49] Figure 7 is a cartoon showing how basal buoyancy might trigger gravitational collapse of an ice sheet. Basal shear stress τ_O is kept constant when $P_W/P_I = 0$ for a frozen bed along a flowband of variable height h_I and constant width w_I, with $x = 0$ at the ice margin, horizontal along the flowband, and positive toward the ice divide. The bed is horizontal for simplicity. An ice sheet lies on a frozen bed and $f_W = 0$ at the ice margin in Figure 7a. The longitudinal gravitational force in ice is $F_I = \bar{P}_I w_I h_I = 1/2\rho_I g w_I h_I^2$ and is balanced by longitudinal shear force at the bed $F_S = \tau_O w_I x$, giving the parabolic profile $x = (\rho_I g/2\tau_0)h_I^2$. Water rises at the ice sheet margin in Figure 7b, causing f_W to increase and calving retreat over length L such that $x = (\rho_I g/2\tau_0)h_I^2 - L$ gives the ice sheet profile upslope from the calving ice wall. Resistance to F_I is now from $F_W = \bar{P}_W w_I h_W = 1/2\rho_W g w_I h_W^2$ for water height h_W, from longitudinal tensile force $F_T = \sigma_T w_I h_I$ for local tensile stress σ_T at the ice wall, and from $F_S = \tau_O w_I x$ between the ice wall and the ice divide. Water rises high enough to float the ice wall in Figure 7c, converting it into a floating ice shelf, so that $f_W = 1$. Force F_I at the grounding line is resisted by F_T and F_S toward the ice divide and F_W at the calving front of the ice shelf, with $P_W/P_I = 0$ for ice grounded along $x > 0$ and $P_W/P_I = 1$ for ice floating along $x < 0$. Basal buoyancy propagates toward the ice divide in Figure 7d, keeping $f_W = 1$ but with $\bar{P}_W$ and h_W decreasing to zero over a distance where $0 < P_W/P_I < 1$ upslope from the grounding line, thereby triggering gravitational collapse by lowering the ice surface in stream flow. Basal buoyancy propagates toward both the ice divide and the ice margin where $f_W = 0$ in Figure 7e, perhaps as surface meltwater reaches the bed through crevasses [*Zwally et al.*, 2002b] in the ablation zone of Figure 7a. Then the ice stream lengthens in both directions, causing gravitational collapse toward the ice divide and extending the ice margin as an ice lobe being uncoupled from the bed. Like extending subglacial Lake Vostok to the sea, a massive ice stream surge would occur when basal thawing beneath the ice lobe reaches the ice margin.

[50] As a final thought, suppose an ice stream floats on a bed of mercury, which has a density $\rho_M \approx 14 \rho_W$. Then (ρ_I/ρ_W) in equation (57) is replaced by $\rho_I/\rho_M \approx \rho_I/14 \rho_W$ and σ_T increases by an order of magnitude. This result is also obtained for $f_W (\rho_I/\rho_W)$ when $f_W \approx 1/14$. Both greatly increase the ice thickness that can move forward to displace air.

References

Andrews, J. T., and K. Tedesco, Detrital carbonate-rich sediments, northwestern Labrador Sea: Implications for ice-sheet dynamics and iceberg rafting (Heinrich) events in the North Atlantic, *Geology*, *20*, 1087–1090, 1992.

Bindschadler, R. A., Actively surging West Antarctic ice streams and their response characteristics, *Ann. Glaciol.*, *24*, 409–413, 1997.

Budd, W. F., P. L. Keage, and N. A. Blundy, Empirical studies of ice sliding, *J. Glaciol.*, *23*, 157–170, 1979.

Budd, W. F., D. Jenssen, and I. N. Smith, A three-dimensional time-dependent model of the West Antarctic ice sheet, *Ann. Glaciol.*, *5*, 29–36, 1984.

Clark, P. U., Surface form of the southern Laurentide Ice Sheet and its implications to ice-sheet dynamics, *Geol. Soc. Am. Bull.*, *104*, 595–605, 1992.

Clark, P. U., Unstable behavior of the Laurentide Ice Sheet over deforming sediment and its implications for climate change, *Quat. Res.*, *41*, 19–25, 1994.

Clark, P. U., Fast glacier flow over soft beds, *Science*, *267*, 43–44, 1995.

Day, C., Warm bedrock forms water beneath rapidly moving ice stream in central Greenland, *Phys. Today*, March 17–18, 2002.

Denton, G. H., and T. J. Hughes, Reconstructing the Antarctic Ice Sheet at the Last Glacial Maximum, *Quat. Sci. Rev.*, *21*, 193–202, 2002.

Drewry, D. J., Antarctica: Glaciological and geophysical folio, report, Scott Polar Res. Inst., Univ. of Cambridge, Cambridge, U. K., 1983.

Echelmeyer, K. A., W. D. Harrison, C. Larsen, and J. E. Mitchell, The role of the margins in the dynamics of an active ice stream, *J. Glaciol.*, *40*, 527–538, 1994.

Engelhardt, H., and B. Kamb, Basal hydraulic system of a West Antarctic ice stream: Constraints from borehole observations, *J. Glaciol.*, *43*, 207–230, 1997.

Fahnestock, M. A., W. Abdalati, I. R. Joughin, J. M. Brozena, and S. P. Gogineni, High geothermal heat flow, basal melt, and the origin of rapid ice flow in central Greenland, *Science*, *294*, 2338–2342, 2001a.

Fahnestock, M. A., I. R. Joughin, T. A. Scambos, R. Kwok, W. B. Krabill, and S. Gogineni, Ice-stream-related patterns of ice flow in the interior of northeast Greenland, *J. Geophys. Res.*, *106*(D24), 34,035–34,045, 2001b.

Fastook, J. L., A map-plane finite-element program for ice sheet reconstruction: A steady state calibration with Antarctica and a reconstruction of the Laurentide Ice Sheet for 18,000 B.P., in *Computer Assisted Analysis and Modeling on the IBM 3090*, edited by K. R. Billingley, H. U. Brown III, and E. Dehoranes, pp. 45–80, Baldwin, Univ. of Georgia, Athens, Ga., 1992.

Greve, R., A continuum-mechanical formulation for shallow polythermal ice sheets, *Philos. Trans. R. Soc. London, Ser. A*, *355*, 921–974, 1997.

Heinrich, H., Origin and consequences of cyclic rafting in the northeast Atlantic Ocean during the past 130,000 years, *Quat. Res.*, *29*, 142–152, 1988.

Hooke, R. L., *Principles of Glacier Mechanics*, 248 pp., Prentice-Hall, Old Tappan, N. J., 1998.

Hughes, T., The West Antarctic Ice Sheet: Instability, disintegration, and initiation of ice ages, *Rev. Geophys.*, *13*(4), 502–526, 1975.

Hughes, T., West Antarctic ice streams, *Rev. Geophys.*, *15*(1), 1–46, 1977.

Hughes, T., Numerical reconstructions of paleo ice sheets, in *The Last Great Ice Sheets*, edited by G. H. Denton and T. Hughes, pp. 221–261, Wiley-Intersci., New York, 1981.

Hughes, T., The Jakobshavns effect, *Geophys. Res. Lett.*, *13*(1), 46–48, 1986.

Hughes, T., On the pulling power of ice streams, *J. Glaciol.*, *38*, 125–151, 1992.

Hughes, T., The structure of a Pleistocene glaciation cycle, in *The Johannes Weertman Symposium*, edited by R. J. Arsenault et al., pp. 375–400, Miner., Metals, and Mat. Soc., Warrendale, Pa., 1996.

Hughes, T., *Ice Sheets*, 343 pp., Oxford Univ. Press, New York, 1998.

Hulbe, C. L., and D. R. MacAyeal, A new numerical model of coupled inland ice sheet, ice stream, and ice shelf flow and its application to the West Antarctic Ice Sheet, *J. Geophys. Res.*, *104*(B11), 25,349–25,366, 1999.

Hütter, K., *Theoretical Glaciology*: *Material Science of Ice and the Mechanics of Glacier and Ice Sheets*, 510 pp., D. Reidel, Norwell, Mass., 1983.

Huybrechts, P., A 3-D model for the Antarctic Ice Sheet: A sensitivity study on the glacial-interglacial contrast, *Clim. Dyn.*, *5*(2), 79–92, 1990.

Huybrechts, P., The present evolution of the Greenland Ice Sheet: An assessment by modelling, *Global Planet. Change*, *9*, 39–51, 1994.

Johnson, J., A basal water model for ice sheets, Ph.D. thesis, Univ. of Maine, Orono, Maine, 2002.

Johnson, J., and J. L. Fastook, Northern Hemisphere glaciation and its sensitivity to basal melt water, *Quat. Int.*, *95–96*, 65–74, 2002.

Joughin, I. R., S. Tulaczyk, R. A. Bindschadler, and S. F. Price, Changes in West Antarctic ice stream velocities: Observation and analysis, *J. Geophys. Res.*, *107*(B11), 2289, doi:10.1029/2001JB001029, 2002.

Kamb, B., C. F. Raymond, W. D. Harrison, H. Engelhardt, M. M. Brugman, and T. Pfeffer, Glacier surge mechanism: 1982–1983 surge of Variegated Glacier, Alaska, *Science*, *227*(4686), 469–479, 1985.

Kamb, B., Basal zone of the West Antarctic ice streams and its role in lubrication of their rapid motion, in *The West Antarctic Ice Sheet*: *Beha-*

vior and Environment, *Antarct. Res. Ser.*, vol. 77, edited by R. B. Alley and R. A. Bindschadler, AGU, Washington, D. C., 2001.

Kwok, R., M. J. Siegert, and F. D. Carsey, Ice motion over Lake Vostok, Antarctica: Constraints on inferences regarding the accreted ice, *J. Glaciol.*, *46*, 689–694, 2000.

MacAyeal, D. R., Large-scale ice flow over a viscous basal sediment: Theory and application to Ice Stream B, Antarctica, *J. Geophys. Res.*, *94*(B4), 4071–4087, 1989.

Mahaffy, M. W., A three-dimensional numerical model of ice sheets: Tests on the Barnes Ice Cap, Northwest Territories, *J. Geophys. Res.*, *81*(B6), 1059–1066, 1976.

Nye, J. F., The flow of glaciers and ice sheets as a problem in plasticity, *Proc. R. Soc. London, Ser. A*, *207*, 554–572, 1951.

Nye, J. F., The mechanics of glacier flow, *J. Glaciol.*, *2*, 82–93, 1952.

Nye, J. F., The flow law of ice from measurements in glacier tunnels, laboratory experiments and the Jungfraufirn borehole experiment, *Proc. R. Soc. London, Ser. A*, *219*, 477–489, 1953.

Nye, J. F., The motion of ice sheets and glaciers, *J. Glaciol.*, *3*, 493–507, 1959.

Orowan, E., Remarks at a joint meeting of the British Glaciological Society/British Rheologists Club, and the Institute of Metals, *J. Glaciol.*, *1*, 231–236, 1949.

Paterson, W. S. B., *The Physics of Glaciers*, 480 pp., Pergamon, New York, 1994.

Raymond, C. F., K. A. Echelmeyer, I. M. Whillans, and C. S. M. Doake, Ice stream shear margins, in *The West Antarctic Ice Sheet*: *Behavior and Environment*, *Antarct. Res. Ser.*, vol. 77, edited by R. B. Alley and R. A. Bindschadler, pp. 137–156, AGU, Washington, D. C., 2001.

Reeh, N., On the calving of ice from floating glaciers and ice shelves, *J. Glaciol.*, *7*, 215–232, 1968.

Robin, G. D. Q., Glaciology III: Seismic shooting and related investigations, in *Norwegian, British, Swedish Antarctic Expedition, 1949–1952*, vol. 5, *Scientific Results*, pp. 111–125, Norsk Polarinst., Svalbard, Norway, 1958.

Thomas, R. H., The creep of ice shelves: Theory, *J. Glaciol.*, *12*, 45–53, 1973a.

Thomas, R. H., The creep of ice shelves: Interpretation of observed behaviour, *J. Glaciol.*, *12*, 55–70, 1973b.

Thomas, R. H., and D. R. MacAyeal, Derived characteristics of the Ross Ice Shelf, *J. Glaciol.*, *28*, 397–412, 1982.

Van der Veen, C. J., A note on the equilibrium profile of a free floating ice shelf, report, 15 pp., Inst. voor Meteorol. en Oceanogr., Rijksuniv.-Utrecht, Utrecht, Netherlands, 1983.

Van der Veen, C. J., *Fundamentals of Glacier Dynamics*, 462 pp., A. A. Balkema, Brookfield, Vt., 1999.

Weertman, J., Deformation of floating ice shelves, *J. Glaciol.*, *3*, 38–42, 1957a.

Weertman, J., On the sliding of glaciers, *J. Glaciol.*, *3*, 33–38, 1957b.

Weertman, J., General theory water flow at the base of a glacier or ice sheet, *Rev. Geophys.*, *10*, 287–333, 1972.

Weertman, J., Position of ice divides and ice centers on ice sheets, *J. Glaciol.*, *12*, 353–360, 1973.

Weis, M., R. Greve, and K. Hutter, Theory of shallow ice shelves, *Continuum Mech. Thermodyn.*, *11*, 15–50, 1999.

Whillans, I. M., Y. H. Chen, C. J. Van der Veen, and T. Hughes, Force Budget III: Application to three-dimensional flow of Byrd Glacier, Antarctica, *J. Glaciol.*, *35*, 68–80, 1989.

Whillans, I. M., and C. J. Van der Veen, The role of lateral drag in the dynamics of Ice Stream B, Antarctica, *J. Glaciol.*, *43*, 231–237, 1997.

Zwally, H. J., B. Schultz, W. Abdalati, J. Abshire, C. R. Bentley, A. Brenner, K. Quinn, S. Palm, J. Spinhirne, and R. H. Thomas, ICESat's laser measurements of polar ice, atmosphere, ocean, and land, *J. Geodyn.*, *34*, 405–445, 2002a.

Zwally, H. J., W. Abdalati, T. Herring, K. Larson, J. Saba, and K. Steffen, Surface melt-induced acceleration of Greenland ice-sheet flow, *Science*, *297*, 218–222, 2002b.

———————————

T. Hughes, Department of Earth Sciences, Climate Change Institute, Bryand Global Sciences Center, University of Maine, Orono, ME 04469-5790, USA. (debbies@maine.edu)